ABSTRACT

OWOYELE, OPEOLUWA OLAWALE. A Corrugated Architecture for Thick Film Thermoelectric Devices. (Under the direction of Dr. Brendan O'Connor).

A novel thermoelectric (TE) device architecture is presented that employs thick film TE elements on a plastic substrate in a corrugated structure sandwiched between planar plastic layers. The corrugated architecture of the TE materials replace the semiconductor legs in a conventional "bulk" TE device. This design is compatible with low cost thick film processing in a roll-to-roll fashion onto plastic substrates making it attractive from a low-cost perspective. In this thesis, first the performance of a single thermocouple of such a device is analyzed and the effect of the parasitic heat losses through the plastic substrate is examined. By using a substrate with a thickness of 70 μm, the parasitic heat transfer is limited to 2.6% when the temperature difference between the hot and cold junctions is 25 K. The single-couple model also shows that using thicker active layers is desirable to achieve more cooling power from a device, and by increasing the thermoelement thickness from 25 μm to 75 μm, the cooling power increases by 217%. While these trends are expected, the model provides a quantitative measure of performance variation with changes in the device dimensions. The performance of an array of such thermocouples is then considered, and the effects of various geometrical parameters of the corrugated architecture are presented. Finally, the heat sink demands of the corrugated TE device are compared to an equivalent bulk device, showing that the proposed device may require less elaborate heat sinks. Combined, the results show that the proposed device may be superior to other TE cooling module designs for applications that require low cooling power densities owing to the potential of low-cost fabrication and reduced heat sink design demands.

A Corrugated Architecture for Thick Film Thermoelectric Devices

by
Opeoluwa Olawale Owoyele

A thesis submitted to the Graduate Faculty of
North Carolina State University
in partial fulfillment of the
requirements for the degree of
Master of Science

Mechanical Engineering

Raleigh, North Carolina

2014

APPROVED BY:

_____	_____
Dr. Scott Ferguson	Dr. Alexei Saveliev

_____
Dr. Brendan O'Connor
Committee Chair

DEDICATION

To *my dad*, for his inspiration and invaluable support

To *my mum*, for her indescribable love and sacrifice

BIOGRAPHY

The Author was born in a Northern Town called Zaria in Nigeria, West Africa on October 5, 1990. Following the completion of his Secondary school education, he enrolled in University of Ilorin, Nigeria, where he obtained his bachelor's degree in Mechanical Engineering. He enrolled as a graduate student in North Carolina State University in January 2013.

ACKNOWLEDGMENTS

I would like to express my gratitude to a number of people, without which this work will not have been possible. First, I would like to express my gratitude to my advisor, Dr. O'Connor for his time, motivation and guidance throughout this thesis. I would also like to thank Dr. Ferguson and Dr. Saveliev for their service on my committee. My appreciation also goes to Tianlei and Margaret for their advice.

Thanks to all my friends for their support, as well as my Oluwatosin for her love and encouragement. I would also like to show appreciation to all my siblings for their support, especially my big brother "Akins", for encouraging and prodding me on throughout this thesis. Specially, I would like express a deep heartfelt gratitude to my Dad for his love and unrepayable support in all areas of my life up until this point, and my sweet Mum whose wise words of advice, motherly love and unrestrained sacrifice has brought me this far. Finally, ultimate thanks goes to my Lord and Savior, Jesus Christ: who was, who is and who is to come – who gives me wisdom and strength for each day; who triumphed over death and conquered the grave.

TABLE OF CONTENTS

LIST OF TABLES

LIST OF FIGURES

LIST OF SYMBOLS

Symbols

A	Cross-sectional Area of thermoelement
Am	Area of thermoelectric module
B	The overall width of thermoelectric module
c	Specific heat capacity at constant pressure
COP	Coefficient of performance
d	Length of a hybrid thermocouple projected into the horizontal plane.
D	Overall length of hybrid thermoelectric module
$\vec{E}$	Electric field intensity vector
h	Average heat transfer coefficient on a surface
H	Height of thermoelectric module
I	Current flowing through the thermocouple
$\vec{\mathrm{j}}$	Current density vector
K	Thermal conductance
l	Length of a thermoelement
n	Number of thermocouples
P	Input electrical power into thermocouple
q_c	Cooling power of a single Thermocouple
$\dot{q}$	Heat generated per unit volume
$\vec{q}$	Heat flux vector
Q_c	Cooling power of an array of thermocouples
R	Electrical resistance
T	Absolute temperature
U	Overall Heat Transfer coefficient
W	Width of a thermoelement
ZT	Dimensionless figure of merit of a TE material

Greek Symbols

α	Seebeck coefficient
γ	Thompson coefficient
δ	Length of contact region
Δ	Change in a property
θ	Angle of inclination of the legs with the horizontal
λ	Diagonal length of one thermoelement in the simplified architecture.
π	Peltier coefficient
ρ	Electrical resistivity
ρ_d	Density of a material
σ	Thermal conductivity
τ	Thickness of a thermoelement

Subscripts

c	Cold side
h	Hot side
max	Maximum
n	n-type semiconductor
p	p-type semiconductor
s	Substrate
∞	Value of a property at ambient conditions

1. Introduction

1.1. Background

The Seebeck effect was discovered by Thomas Seebeck in 1821 who observed that a voltage develops in a material when there is a temperature gradient across the ends of the material [1, 2]. About 13 years after this, Peltier discovered that the reverse is also true [3]. Heat is absorbed or released at the junction of two dissimilar materials when a current is made to flow through it [3—5]. In 1851, Lord Kelvin Thomson used the principles of thermodynamics and energy conservation to establish the relationship between the Peltier and Seebeck effect [2—4]. He also discovered a third phenomenon, called the Thomson effect, which is small compared to the other two effects and states that heat will either be absorbed or released when a temperature gradient and a flow of current exists in a conductor [3, 4]. These initial findings led to the development of thermoelectric devices, which convert heat into electricity or convert electrical power into a temperature gradient [6—8].

Thermoelectric materials can function as electrical generators, heat pumps or refrigerating devices depending on the electrical and thermal boundary conditions, the direction of current flow and the properties of the materials [8—10]. Thermoelectric devices possess a number of advantages over other energy conversion technologies such as the absence of moving parts, low maintenance, environmental friendliness and the potential for precise temperature control [8, 10, 11]. An illustration of a typical thermoelectric device is given in **Figure 1**, and consists of p-type and n-type thermoelectric semiconductor materials connected electrically in series and thermally in parallel. When used in a TE device, these p-type and n-

type materials are referred to individually as thermoelements [12, 13]. The relationship between the electrical potential difference and the temperature gradient in these materials is determined by a property called the Seebeck coefficent. The Seebeck coefficients of p-type and n-type materials are positive and negative respectively and these indicate the direction of the voltage potential that develops under a temperature gradient.

Different architectures for optimizing thermoelectric devices have been used depending on the density of the heat flux and the available space. This ranges from conventional *bulk* structures which absorb heat fluxes as high as a few W/cm^2, to *cross-plane* thin film and thick film devices which have been used in micro-applications such as microprocessor on-chip cooling which dissipate heat fluxes as high as hundreds of W/cm^2 [5, 14—16]. However, cross-plane TE devices suffer from a loss in performance due to parasitic thermal and electrical contact resistances in the system [14—16]. This is because of their extremely short active elements which makes the relative effect of electrical contact resistance more important [15, 17]. There are also *in-plane* thin film and thick film thermoelectric cooling devices that have been shown to be useful in cooling infrared detectors, solid-state lasers, low-noise amplifiers and resonant micro-electromechanical systems where the power dissipation is low and the device performance is significantly enhanced when maintained below room temperature [13, 18—20]. In in-plane architectures, a common loss is due to the supporting substrate which results in a thermal bypass through the substrate [13, 18, 21].

In general, the term thin film TE devices are applied to devices with a thickness of less than 10 μm, while thick film TE devices generally range from 10 μm to 100 μm [22—25]. The principles of operation and applications of these TE device designs are further discussed in

Section 1.2.1. Another important advantage of TE devices is that they can be scaled down to smaller sizes, and the cooling power absorbed by the device remains approximately the same as long as the ratio of the cross-sectional area to the length of the thermoelements remain constant [10].

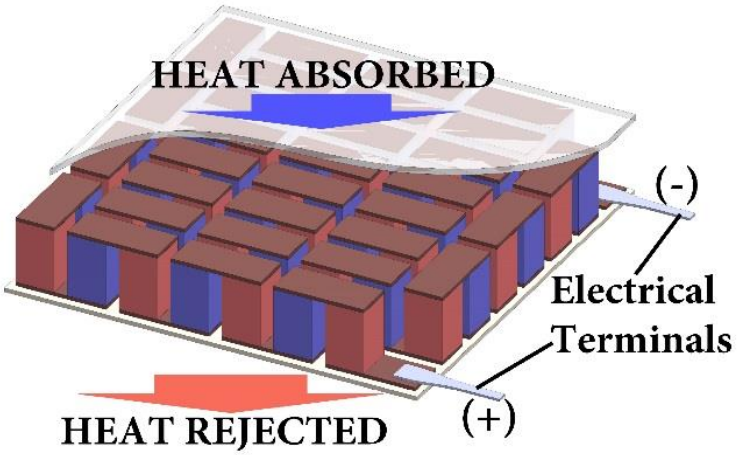

Figure 1: A typical bulk thermoelectric cooling module. The n-type and p-type thermoelements are red-colored and blue-colored respectively in the figure.

1.2. Thesis Overview

1.2.1. Previous Work and Present Applications

A material's potential to perform efficiently in thermoelectric applications is largely determined by a parameter called the dimensionless figure of merit given by [26, 27],

$$ZT = \frac{\alpha^2 T}{\rho\sigma}, \tag{1.1}$$

where ρ is the electrical resistivity while σ is the thermal conductivity of the material. α is the Seebeck coefficient while T is the absolute temperature. The thermal conductivity has two contributions and is given by $\sigma = \sigma_e + \sigma_l$, where σ_e and σ_l are the electronic and lattice contributions to the thermal conductivity respectively. In the development of better thermoelectric materials, the thermal conductivity must be reduced while the electrical conductivity must be increased. This presents a problem, as both current and heat flow are facilitated by mobility of charge carriers in materials [5, 28, 29]. Therefore, research has focused on reducing the lattice contribution to the thermal conductivity of materials [5, 30].

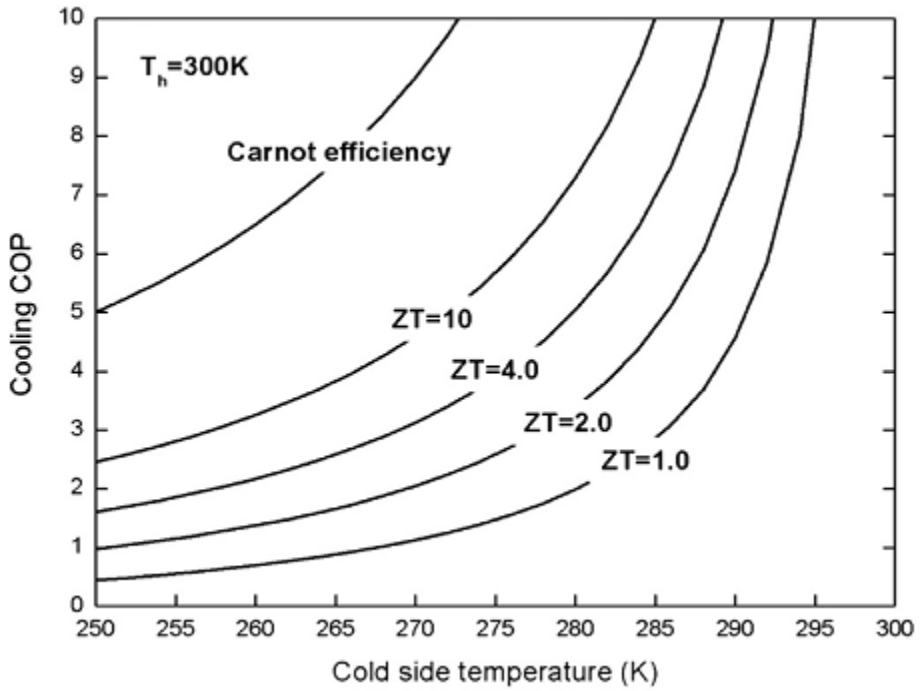

Figure 2: The dependence of COP on the Cold side temperature of the device for different values of ZT from Ref [30].

The dependence of the potential of thermoelectric devices on *ZT* is shown in **Figure 2**. In the figure the hot side temperature, T_h is fixed and it can be seen that in order to increase the *COP* to values closer to the Carnot efficiency, materials with higher *ZT* are needed. Compared to conventional fluid-based cooling technologies, current bulk devices which have a $ZT \sim 1$ at room temperature are not competitive, in terms of their *COP* [5, 30].

Notwithstanding this limitation, thermoelectric devices have been of great importance in niche applications such as cooling of solid-state lasers, power generation or space exploration, portable refrigerators and coolers, picnic baskets, and in medical, scientific and laboratory applications [8, 28, 30]. Also, they have been applied to cooling of electronic devices and to automobiles where they have been used for heating and cooling of seats and mini-refrigerators [8, 30]. Recently, work has been also done in applying them to domestic air-conditioning systems [30].

The type of architecture used for TE devices depends on how much heat flux needs to be absorbed and how much space is available. Therefore, due to manufacturing difficulties in scaling down bulk TE elements, thin film and thick film devices are typically used in micro-applications. Also, the cooling power density of a TE device depends on the aspect ratio of its thermoelements, and a larger cross-sectional area to length ratio results in increased cooling power. Therefore, applications requiring low heat fluxes typically use in-plane films, while cross-plane films are employed when very high cooling power densities are required.

1.2.1.1. Space Cooling and Refrigeration

Conventional fluid-based technologies such as vapor-compression and vapor-absorption systems are typically bulky. Thus for applications requiring portability and little space they are generally unsuitable. Thus, TE devices have found widespread applications in portable vaccine coolers for remote locations, picnic baskets and mini-refrigerators in vehicles [8, 30]. Although the *COP* is still typically lower than vapor-compression systems, their quietness in operation, compactness and lightweight make them suitable for such applications [8, 28, 30]. Also in refrigeration, vapor-compression systems can have a fluctuation of inner temperature because the compressor switches on and off intermittently to regulate inner temperature [30, 31]. However, a thermoelectric and vapor compression hybrid refrigerator has been evaluated and the results indicate that the oscillation of the inner temperature is always lower than 0.4 ^{o}C [31], which indicates that TE devices are suitable for refrigerating items or components sensitive to fluctuations in temperature.

Solar-powered TE refrigerators have also been designed and investigated experimentally, and results have indicated that the temperature of the refrigeration was reduced from 27 ^{o}C to 5 ^{o}C in approximately 44 min [32].

1.2.1.2. Cooling in Electronics

In electronics, TE devices have been use in cooling of PC processors where the heat flux can be as high as hundreds of Watts per cm^3 [15, 28]. In such cases, the TE cooler is required to cool a component that has a temperature above the ambient temperature by pumping heat away [28]. For reliable operation, in many cases the junction of the electronic

component needs to be maintained at below 85 ^{o}C [30]. Since conventional vapor compression systems are too big, cross-plane thin film or thick film TE devices are usually employed in such systems [15, 30].

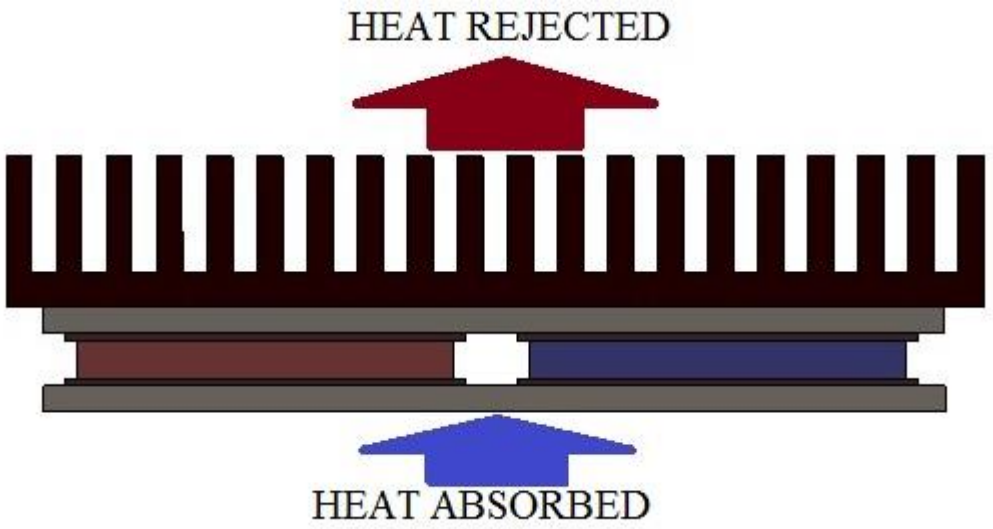

Figure 3: A schematic showing the operation of a cross-plane thin or thick film TE device.

An illustration of such a device is shown in **Figure 3** where it can be seen that heat transfer and current flow occurs perpendicular to the plane of the film. These devices are relatively very thin and small and hence they are able to fit into micro-electronic packages and absorb hundreds of W/cm^3 to meet up with the heat dissipated by such electronic devices [15, 30].

On the other hand, TE devices have also been used to reduce thermal noise and leakage current in electronic devices. An example of this is in the cooling of CdZnTe detectors which are used for X-ray astronomy where the energy resolution of such systems is improved by

cooling the detector to temperatures between -30 ^oC to -40 ^oC [8]. In-plane thermoelectric devices have high aspect ratios where current flows laterally along the film and are widely used in applications involving low heat fluxes which includes stabilization of laser diodes, reduction of noise in integrated circuits, and the cooling of infrared detectors [13, 18, 19]. The application an in-plane thin film device has been explored, where a TE array was used in cooling an infrared component [13]. The schematic of this is shown in **Figure 4**, where the device is arranged such that the cold junctions surround the cooled infrared component, while the hot junctions are at the edges of the device [13].

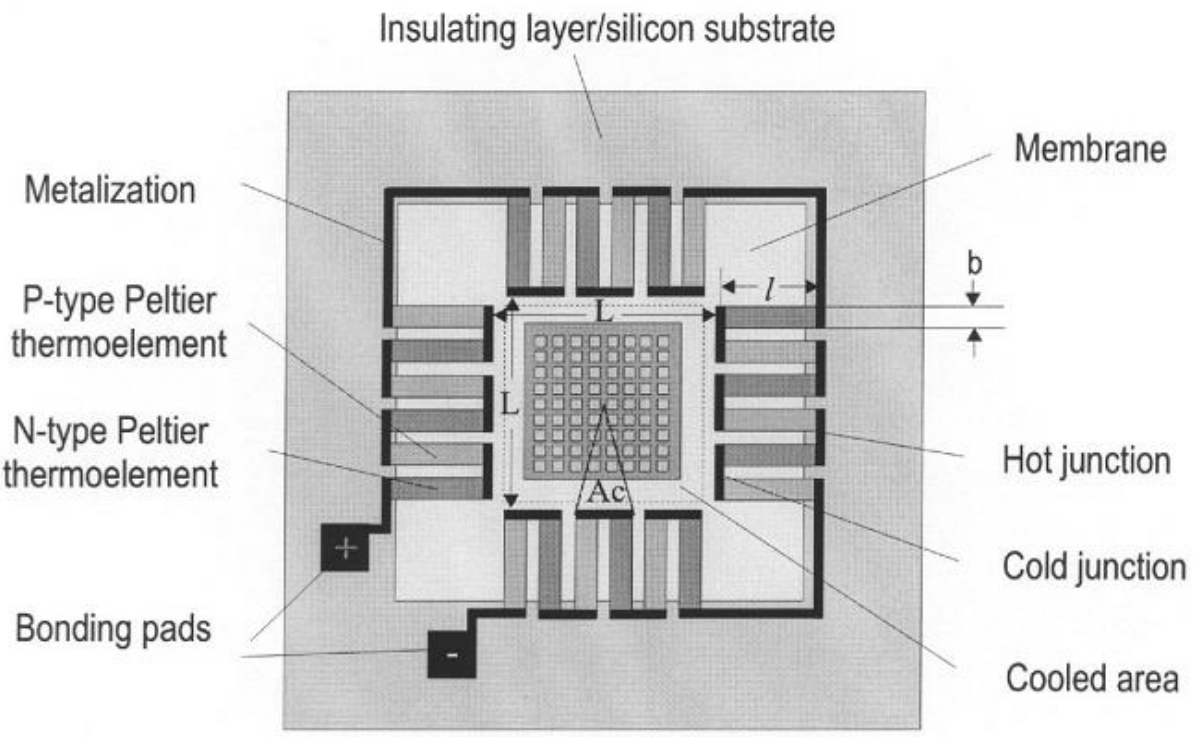

Figure 4: A schematic showing infrared components cooled by an integrated in-plane thin film thermoelectric cooler from Ref [13].

In-plane TE devices typically need a supporting substrate on which the thermoelements rest, and in this case a silicon substrate was used [13]. By using a thermoelement length of 0.15 *mm* with a thermoelement and substrate thickness of 2 μm, the device performance was 40% of that of a free standing device when the difference between hot junction and cold junction temperatures was 25 *K* [13]. This drop is in performance is due to parasitic heat conduction through the substrate from the hot junction to the cold junction. Thus, it can be seen that a major setback in the use of in-plane thin film and thick film devices is the parasitic heat conduction through the substrate which creates a large drop in performance. It was also found that the device could cool at a power of 1 *mW* with a *COP* of 0.6 when the temperature difference was 20 *K* [13].

1.2.1.3. Body Cooling Applications

Thermoelectric devices have also been applied to systems involving body cooling. This is a broad category, as they have been used for body cooling in domestic outdoor, medical, and automobile applications. For body cooling in domestic outdoor applications, a solar-powered thermoelectrically cooled headgear has been developed for use in harsh conditions and this will be discussed in greater detail in **Section 3.5** [33]. The use of TE devices integrated into clothes for industrial workers working in hot environment has also been discussed [34]. In medical applications, a digital array of micro-coolers to locally cool tissues in order to stop bleeding due to micro-cuts, thereby helping doctors reduce the risk of complications during surgery has been developed [35].

In automobile body cooling applications, TE devices have been used in the cooling and heating of car seats, and temperature control system for such a device has been developed [36]. TE devices incorporated into steering wheels, gear shift knobs, door handles, carpets, and armrests, as well as truck seats for the purpose of overall thermal comfort of truck drivers are presently on the market [30, 37, 38].

1.2.2. Motivation

Many bulk TE devices have found usefulness in applications where a relatively high cooling rate per unit area is needed because for some of these applications, conventional cooling technologies cannot sufficiently dissipate such heat fluxes [32]. While this has certainly been the case in many applications, TE devices have required usage in commercial applications where their lightness, compactness and reliability have been needed, but where the cooling density demands have been relatively lower [39, 40]. Such cases have led to the incorporation of elaborate heat sink designs which in some cases includes fins and fans at both the hot and cold sides of the TE module [30, 39, 40]. Such a design adds to the cost a module, presents an additional design problem to be solved in the development of a TE module and incorporates moving parts into the system, which undermines reliability. Also, if a fan is included the overall *COP* of the system is reduced as some additional electrical power will be required to drive the fan.

Also, the power consumption of a TE cooler is partly determined by the ratio of its cross-sectional area to its length. As it will be shown in a **Section 2.2**, using a device with thinner cross-sections while keeping length constant is necessary to reduce the cooling power

density of a TE thermoelement. Thus, in-plane thin film or thick film devices could present a better option for cooling in such applications as those requiring low cooling density. However, no design exists currently to laterally populate these films on larger areas, such as exists for bulk modules. Although in-plane thin and thick film devices have been used in micro-applications involving low heat dissipation [8, 13], they are yet to be used in applications involving larger areas, such as will be explored in this thesis.

In addition to this, as reported in **Section 1.2.1**, in-plane thin film devices suffer from a great loss in performance and this can make the actual device performance as low as 40% of that of a free standing device, in terms of cooling power [13]. As mentioned earlier, this is as a result of an increased overall thermal conductance of the device due to the parasitic thermal conduction through the substrate. Because the hot junction is maintained at a higher temperature than the cold junction, a potential for heat transfer is set up, and heat flows from the hot junction to the cold junction. This presents an unwanted phenomenon which partially offsets the heat absorbed at the cold junction [13, 19]. Thus an in-plane thin film or thick film device that is implemented for larger area applications must possess minimal thermal bypass performance losses.

Therefore a device design is needed for use in applications requiring low heat flux dissipation, which also possesses typical advantages of TE devices such as low weight and compactness. Such a device will need to have to have a relatively thin cross-sectional area, and thus will need to be supported by a substrate. In doing this, the conventionally high losses through the substrate will need to be kept low enough to justify the practical implementation of such a device.

1.2.3. Research Objectives

The objective of the thesis is to explore a hybrid thermoelectric cooler (H-TEC) architecture that consists of thermoelectric films printed on a thin corrugated plastic substrate that is sandwiched between two plastic plates, illustrated in **Figure 5**. This design represents a hybrid of conventional bulk thermoelectric devices and in-plane thick film thermoelectric designs. As stated in the **Section 1.2.2**, in-plane thin and thick films are suitable for low cooling power density applications, but no design exists to populate them laterally on larger areas and so their use has been limited to micro-applications. Thus the objective of this thesis is to explore a corrugated architecture for the purpose of applying thick film TE properties on a larger area.

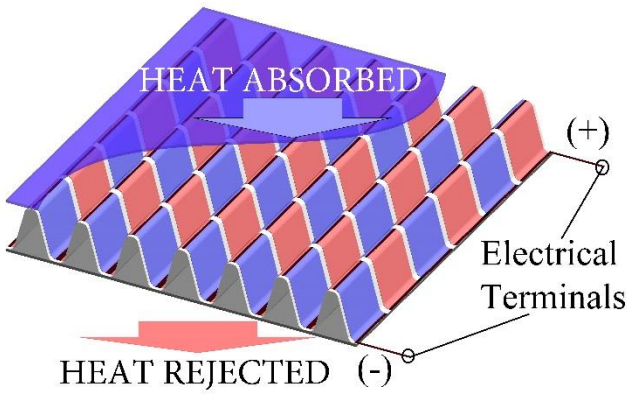

Figure 5: The architecture of the novel corrugated thermoelectric device structure. The n-type and p-type thermoelements are red-colored and blue-colored respectively in the figure.

The performance of the structure is theoretically analyzed from a single thermoelectric couple to a thermoelectric cooler module showing this architecture is beneficial in applications

where a low heat flux is required over a relatively large area. We show that with geometric optimization, such a device will require a less elaborate heat sink design as compared to a bulk design. The device also will have comparable coefficient of performance, by minimizing the parasitic heat losses through the substrate.

Prior to this work, to the best of our knowledge the application of thin and thick film TE devices has been restricted to micro-coolers where low heat dissipation is required and to microgenerators such as in sensor applications [19, 20]. Here, we show that with a suitable thermoelectric architecture, thick film thermoelectric materials have potential advantages for large area applications with competitive system performance and reduced system costs.

1.2.4. Summary of Results

- Generally, the losses through the substrate are low and the *COP* is comparable to that of a bulk device. At an optimum current of 0.526 A and a cold junction temperature of 270 K, the cooling power of a single 75 μm thick thermocouple was 23.6 mW, which represents 97% of the performance of a free standing device. The cooling power increases with increasing cold junction temperature and increasing thermocouple thickness. Also, the *COP* of such a device at the same boundary temperatures is 1.06 at the optimum current of 0.15 A, comparable to that of a representative bulk device which is about 1.19.
- In addition to its dependence on the thermocouple properties, the performance of the hybrid thermoelectric cooling module (H-TECM) depends largely on the angle of inclination of the p-type and n-type thermoelements and how blunt or sharp-pointed

the contact regions are. The dependence becomes more pronounced as the angle of inclination of the legs approach 90^{o}.

- The Hybrid Thermoelectric Cooling Module (H-TECM) can produce a reasonable cooling power even in the absence of a cold side heat sink. Thus, by using air-cooled and water-cooled cold sides in natural convection a representative H-TECM can deliver a cooling power of 3.4 *W* and 5.16 *W* respectively.

1.3. Theory

1.3.1. Seebeck Effect

As stated earlier, the Seebeck effect postulates that a voltage potential develops across a conductor if there is a temperature gradient across it. **Figure 6** shows a schematic representation of this effect from Ref [2].

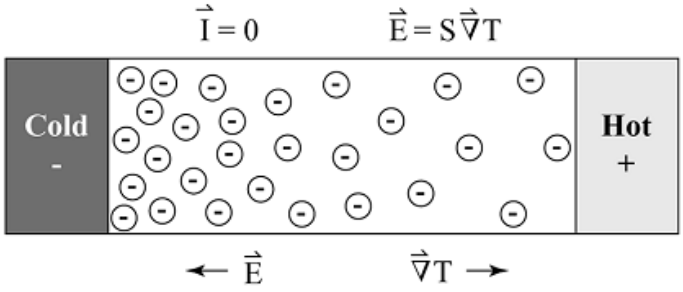

Figure 6: A simplified illustrative diagram from Ref [2] showing the change in concentration of classical charged particles in a chamber when a temperature difference is sustained between the ends.

This case represents a simplified analogy where a chamber is filled with negatively charged particles and one end of the chamber is maintained at a higher temperature than the other end. In the presence of such a temperature gradient, there will be a net diffusion of charged particles from the hot side to the cold side and this will lead to an electric field with a direction opposite to the temperature gradient [2].

The Seebeck effect is mathematically given by [2],

$$\alpha = \lim_{\Delta T \to 0} \frac{\Delta V}{\Delta T}, \tag{1.2}$$

where ΔT and ΔV are the temperature difference and the voltage difference, respectively. An illustration of the Seebeck effect in a power generation device is given in **Figure 7b** [5].

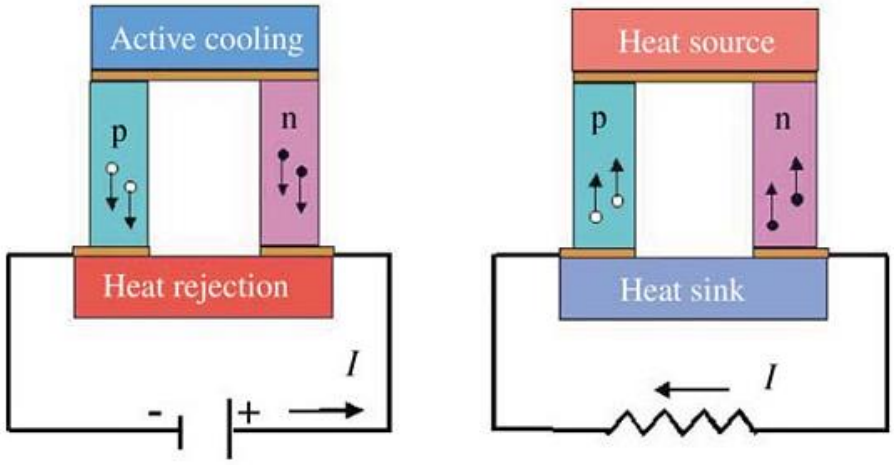

(a) (b)

Figure 7: A schematic illustrating the operation of a thermocouple in (a) heating, and (b) power generation mode as obtained from Ref [5]. The open circles represents holes while the closed circles represents electrons.

A heat source at one end of the device causes a “drift” of electrons in the n-type material and holes in the p-type material towards the heat source and produces a potential difference which leads to a flow of current [5].

1.3.2. Peltier Effect

It is possible to achieve cooling from a thermoelectric module by passing a current through the device as shown in **Figure 7a** [5]. Due to the difference in Fermi energy levels of two materials, the electrons traveling through the interface either have to move to a lower or higher energy level, which constitutes a macro-scale heat release or heat absorption respectively [5]. Thus, as illustrated in **Figure 8**, a junction can either reject or absorb heat depending on the current flow and the properties of the two materials [5].

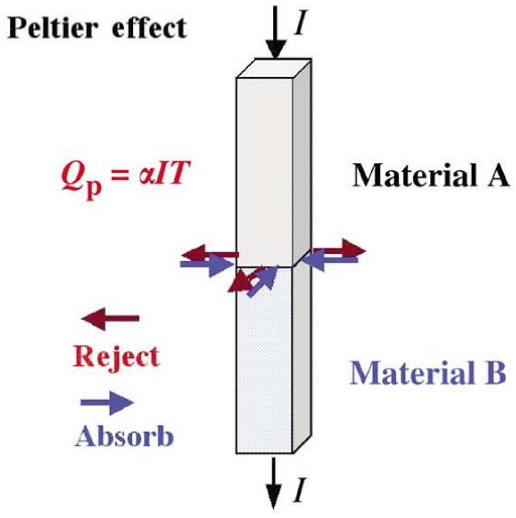

Figure 8: A schematic illustrating the Peltier effect between the junction of two dissimilar materials.

The magnitude of the cooling or heating at the junction is described by the Peltier coefficient which is given by [2],

$$\pi = \frac{q_c}{I}, \tag{1.3}$$

where q_c is the rate of cooling and I is the current.

1.3.3. Thomson Effect

The Thomson effect influences the thermoelectric performance of a device when we have a material with a temperature-dependent Seebeck coefficient [6, 41]. The Thomson coefficient is the reversible change in heat energy per unit current flow per unit temperature gradient [4]. Therefore, the Thomson coefficient (γ) is given by [2],

$$\gamma = \lim_{\Delta T \to 0} \frac{\Delta q}{I \Delta T}. \tag{1.4}$$

In addition to this, Lord Kelvin derived the relationships between the Seebeck and the Peltier coefficients to be given as [2],

$$\frac{d\alpha}{dT} = \frac{\gamma}{T}, \tag{1.5}$$

$$\pi = \alpha T. \tag{1.6}$$

Thus the Peltier heat absorbed at a junction is given by [5],

$$q_c = \pi I, \tag{1.7}$$

$$\therefore q_c = \alpha I T. \tag{1.8}$$

1.3.4. Governing Equations

The equations that govern the behavior of thermoelectric device have been covered in many papers [6, 41, 42, 43]. Here, a brief review of these equations is provided. The general 3-D conduction heat transfer equation is given by [10],

$$\rho_d c \frac{\partial T}{\partial t} = \dot{q} - \vec{\nabla} \cdot \vec{q}, \tag{1.9}$$

where, ρ_d is the density, c is the specific heat of the conductor, t represents time, $\dot{q}$ is the heat generation per unit volume, and $\vec{q}$ is the heat flux vector. For steady state conditions, the temperature of the device is constant with time, and therefore, **Equation 1.9** reduces to [6, 10],

$$\dot{q} = \vec{\nabla} \cdot \vec{q}. \tag{1.10}$$

In an electrical conductor, the heat flux term is given by [6],

$$\vec{q} = \alpha T \vec{\jmath} - \sigma \nabla T, \tag{1.11}$$

where $\vec{\jmath}$ is the current density. Substituting **Equation 1.11** into **Equation 1.10** gives us the following [6],

$$\nabla \cdot (\sigma \nabla T) - \nabla \cdot (\alpha T \vec{j}) + \dot{q} = 0. \tag{1.12}$$

The rate of heat generated is a combination of the joule heating and the Peltier effect. The law of conservation of energy means that since no energy is created, the electrical energy must be expended in overcoming electrical resistance to current flow or doing work against the Seebeck field. This gives us [10],

$$\dot{q} = \vec{\jmath} \cdot \vec{E} = j^2 \rho + \vec{j} \cdot \alpha \vec{\nabla} T, \tag{1.13}$$

where $\vec{E}$ is the electric field intensity vector. The current density vector, $\vec{\jmath}$ is given by [6],

$$\vec{\jmath} = \frac{1}{\rho}\left(\vec{E} - \alpha\nabla T\right). \tag{1.14}$$

An evaluation of **Equation 1.5** also shows that the Thomson coefficient is given by [6, 43],

$$\gamma = T\frac{d\alpha}{dT}. \tag{1.15}$$

Substituting **Equation 1.13** into **Equation 1.12**, by replacing $\dot{q}$ in **Equation 1.12** and simplifying gives [6],

$$\sigma\nabla^2 T - \vec{j}\gamma\nabla T + j^2\rho = 0. \tag{1.16}$$

Equation 1.16 is a second order differential equation. If it is assumed that the Thomson coefficient is constant or the Seebeck coefficient is not a function of temperature, and a further assumption of a 1-D heat and current flow is made, **equation 1.15** can be simplified to the following [10],

$$\frac{d^2T}{dx^2} + \frac{I^2\rho}{A^2\sigma} = 0, \tag{1.17}$$

where *A* is the cross sectional area and is perpendicular to current and heat flow and *x* is the distance along the length of the device in the heat flow direction. Also, based on this 1D assumption, at $x = 0$ **equation 1.11** simplifies to,

$$q_c = \alpha T_c I - \sigma A\frac{dT}{dx}\Big|_{x=0}, \tag{1.18}$$

where q_c is the heat flux at $x = 0$ which corresponds to the cold junction of the device. The temperature profile in **Equation 1.18** can easily be obtained by solving the second-order differential equation in **Equation 1.17**. By setting $x = 0$ for the temperature profile obtained, we can substitute this into **Equation 1.18** to obtain the following,

$$q_c = \alpha T_c I - 0.5\, I^2 \frac{\rho\, l}{A} - (T_h - T_c)\frac{\sigma A}{l}. \tag{1.19}$$

where l is the length of the device, T_h and T_c are the hot and cold junction temperatures respectively. The above equation represents the simplified model of the total cooling power at the cold junction for a thermocouple where the Thomson effect has been ignored. This assumption is reasonable in many cases, but the Thomson effect becomes more important to consider when high temperature gradients exist in the device. The 1-D heat conduction assumption is also reasonable if we have negligible conductive and radiative heat losses from the lateral surfaces of the thermocouple legs. The equation arrived at by assuming a 1-D heat conduction and a constant Seebeck coefficient have been shown to predict the performance of thermoelectric generating and cooling devices with a high level of accuracy at relatively low temperatures [6, 10, 44, 45]. These equations will thus be used to analyze the proposed novel thermoelectric device structure.

The cooling power of a single thermocouple and an array of thermocouples at its cold end are given by [10, 13, 23],

$$q_c = I\alpha T_c - K(T_h - T_c) - 0.5 I^2 R, \tag{1.20}$$

$$Q_c = n.\, q_c. \tag{1.21}$$

In **Equation 1.21**, *n* is the number of thermocouples in a module while Q_c is the total cooling power of the array. Also, to find the *COP* of such a device, we need to account for the power input. The power input, *P* and the *COP* are,

$$P = \alpha I(T_h - T_c) + I^2R, \tag{1.22}$$

$$COP = \frac{Q_c}{P}. \tag{1.23}$$

In the above equation, *K* and *R* are the overall thermal conductance and the overall electrical resistance of the device. These two, along with the seebeck coefficient of a single thermocouple are given by,

$$K = \rho_p \frac{\tau_p W_p}{l_p} + \rho_n \frac{\tau_n W_n}{l_n}, \tag{1.24}$$

$$R = R_p + R_n = \sigma_p \frac{l_p}{\tau_p W_p} + \sigma_n \frac{l_n}{\tau_n W_n}, \tag{1.25}$$

$$\alpha = \alpha_p - \alpha_n. \tag{1.26}$$

In Equations **1.24 and 1.25**, τ is the thickness of the thermocouple while *W* represents the width, with the subscripts *p* and *n* denoting the p-type and n-type thermoelements respectively. For a thermoelectric module, in terms of the ambient temperature at the cold side $T_{\infty,c}$, the Overall coefficient of heat transfer into the cold side *U*, and the area of the module available for heat transfer A_m, the cold side temperature is given by,

$$T_c = \frac{UA_m.T_{\infty,c} + n(0.5I^2R + KT_h)}{n(I\alpha + K) + UA_m}. \tag{1.27}$$

2. Proposed Device Architecture

2.1. Device Architecture

In the proposed H-TEC architecture, the p-type and n-type thermoelements are printed on top of the wave-structured substrate in an alternating fashion. This results in thermoelectric legs analogously patterned to the conventional bulk thermoelectric structure, illustrated in **Figure 1**, **Figure 5** and **Figure 9**. This wave structure presents a viable architecture which can be used to arrange thick or thin films on larger areas. For practical implementation, it may be easier to avoid sharp corners associated with a corrugated design. This would eliminate potential areas of mechanical and electrical failure and possibly minimize any electrical resistance issues. In order to analyze the effect of the geometric parameters, the architecture is simplified by approximating the sinusoidal shape as trapezoidal with straight thermoelectric elements as shown in **Figure 9**.

Major module dimensions include the total length D, height H, and width, B. In addition, the length of the contact region of the thermoelectric element with the planar thermal interface layer is given by δ, and the angle between the legs and the horizontal is given by θ. It is assumed that both the p-type and n-type legs have the same dimensions. To provide uniform cooling and to optimize the potential of a device, p-type and n-type materials with similar ZT and dimensions are desirable. This is due to the fact that for different material geometrical properties, the maximum cooling power occurs at different currents as will be shown in **Section 3**. Therefore, it is important that the optimum current of the p-type and n-type material are as close as possible since the same current has to flow through them, and to

this end both semiconductors should have similar geometries and thermoelectric material properties.

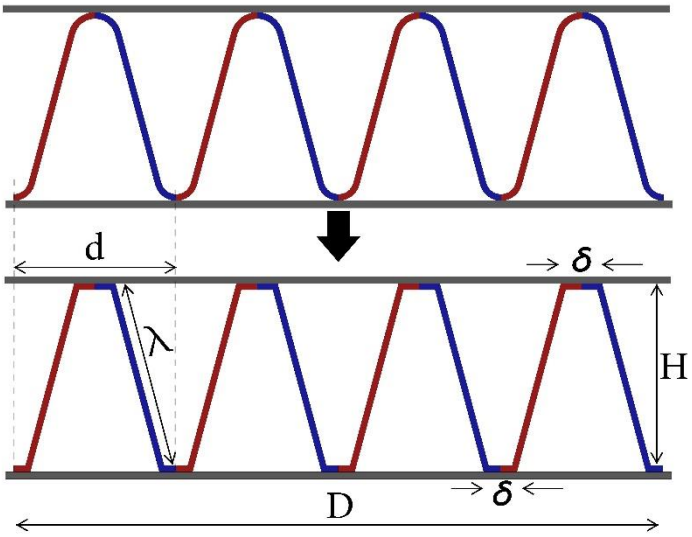

Figure 9: An illustrative diagram showing the simplification made in order to perform a geometrical analysis on the device.

In analyzing such a device, it is important to know the areal fill factor, or thermoelectric cross-sectional area relative to the total cross-sectional area of the device. The areal fill factor will give the information needed to calculate the cooling power density and subsequently the heat sink demands. If we consider an array of thermoelectric elements with a total length *D*, we can arrive at an equation, which describes the number of thermocouples that can fit into a given area per unit width as a function of the angle between the legs and the horizontal, θ. Geometrically, the length of one thermocouple projected to the horizontal is given by,

$$d = \delta + [\lambda cos\theta + \tau sin\theta], \quad (2.1)$$

where λ is the diagonal length of the thermoelement and $\tau = \tau_p = \tau_n$ is the thickness of the active thermoelectric materials. The number of thermocouples in a length *D* is therefore given by,

$$n = \frac{D}{2[\delta + (\lambda cos\theta - \tau sin\theta)]}. \tag{2.2}$$

From **Equation 2.2** it can be seen that the relative importance of the thickness of the thermoelement depends largely on the angle of inclination of the legs. Although the analysis above does not take into consideration the number of thermoelements along the width of the module, this can be easily done by choosing a spacing between elements along the direction of their width and dividing the sum of this spacing and the width of one thermoelement by the total width of the module.

2.2. H-TEC Operation Characteristics

For a thermoelectric cooler, the cooling power, the coefficient of performance, and the maximum temperature difference between the hot and cold junctions are the common performance metrics to be optimized depending on the application [6, 10, 13, 14, 46]. The governing equations used to determine these values have been extensively covered in several papers [10, 47, 48] and described in **Section 1.3.4** for a conventional bulk TE device. However, for the H-TEC the total conductance will be given by,

$$K = \rho_p \frac{\tau_p W_p}{l_p} + \rho_n \frac{\tau_n W_n}{l_n} + 2\rho_s \frac{\tau_s W_s}{l_s}, \tag{2.3}$$

where the subscript *s* denotes the substrate. In the proposed H-TEC design, the thermoelectric materials will be on a plastic substrate and adhered to a plastic thermal interface, therefore the additional third term in **Equation 2.3** is the thermal conductance due to the existence of the

plastic substrate. In this analysis the following commonly applied assumptions are made: (1) Constant material properties, (2) Negligible contact resistances, (3) Thompson effects can be ignored, (4) Effects of convection and Radiation are ignored. While materials properties will change with temperature, assumption (1) and (3) are valid at the temperature range being considered here. Assumption (2) can be made because we are dealing with relatively long thermoelement legs, and assumption (4) is reasonable if we also assume such a device operates in a vacuum and that the temperatures involved are relatively low thereby reducing the effects of convection and radiation respectively. In this analysis, it will also be assumed that the curved thermoelements can be modeled as flat legs as shown in **Figure 10** and this will be shown to be reasonable in **Section 3.3**.

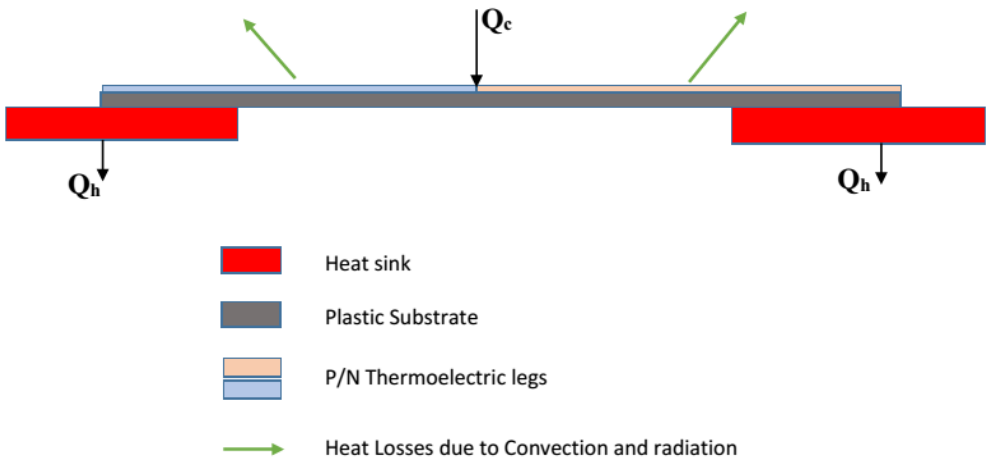

Figure 10: Schematic showing the side view of an in-plane thick film device with flat thermoelements

To compare the bulk thermoelectric cooler (B-TEC) design to the H-TEC design, we can consider the effect of slicing a free-standing bulk thermoelement into thinner cross-

sections. This analysis will show us what happens when we reduce the volume of a thermoelement while keeping length constant. The optimum current in the analysis below is the current which produces maximum cooling power. In general the current that produces maximum cooling power, $Q_{c,max}$ for a given device geometry and properties is given by [47],

$$I_{opt} = \frac{\alpha T_c}{R}. \tag{2.4}$$

Since $R \sim \frac{1}{A}$ and $K \sim A$, we can show by substituting **Equation 1.31** into **Equation 1.20** that,

$$Q_{c,max} = a.A - b.A - c.A, \tag{2.5}$$

where *a*, *b* and *c* are constants and *A* is the cross-sectional area of the thermoelements.

$$\therefore Q_{c,max} \propto A \tag{2.6}$$

Here, it is clearly seen that the maximum cooling density possible for a given thermocouple is linearly proportional to the cross section area of the thermoelements.

2.3. Numerical Solution Setup

The analytical results obtained using the simplified governing equations obtained in **Section 1.3.4** were compared to Numerical results obtained using SOLIDWORKS® 2013 (Dassault Systèmes SolidWorks Corporation, Waltham, MA) and ANSYS® WORKBENCH™ v14.5 (ANSYS Inc., Canonsburg, PA). A particular emphasis was placed on comparing the curved sinusoidal legs structure to a simplified case of a flat thermoelectric couple on a plastic substrate. Model 1 represented the real design with curved tops and bottoms. The overall dimensions are identical to that of the analytical device, featuring an overall length of 15 *m*m,

a thermocouple thickness of 75 μm and a substrate with a thickness of 70 μm. The chosen parameters are descriptive of a representative system, and are selected for the purpose of analyzing the potential performance of the H-TEC design. As stated in **Section 2.1**, the analytical solution ignored the curved regions and assumed flat thermoelements. To compare the effect of this simplification, a second model was developed that considered straight thermoelectric elements (similar to the trapezoidal approximation) as illustrated in **Figure 11b**.

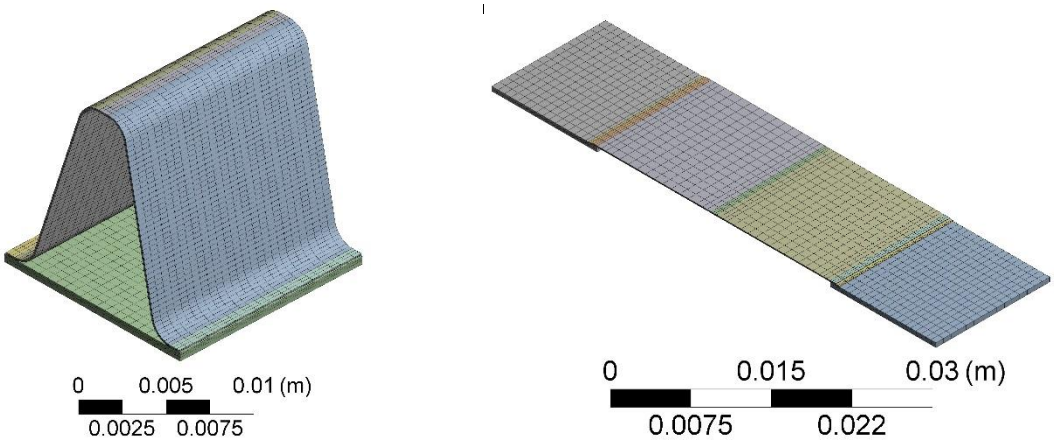

(a) (b)

Figure 11: Picture of the thermoelectric models constructed in SOLIDWORKS® and ANSYS® WORKBENCH™. The models are for, (a) the expected sinusoidal stucture that would be employed commercially, and (b) the simplified flat thermoelectric elements. The images also show the finite element mesh created to numerically analyze device performance.

The models constructed in SOLIDWORKS® were imported into the commercial software, ANSYS® WORKBENCH™, which has a built-in function to solve thermoelectric problems. These two geometries are shown in **Figure 11**. When the grid system was set up, the total number of elements was 9,594, with 52,523 nodes for the H-TEC design model while

the model with flat legs had 3,315 elements and 16,257 nodes. Further refinement of model 1 to 34,000 elements and model 2 to 5,628 elements produced a change in cooling power of less than 0.2% in both cases. The results obtained for the two models are described in detail in **Section 3.3**, showing good agreement between the sinusoidal and flat thermoelement patterns.

3. Results and Discussions

3.1. Single Thermocouple Characteristics

The performance (q_c and *COP*) of a single thermocouple, similar to that illustrated in **Figure 10** is shown as a function of current for different values of T_C in **Figure 12a** and **Figure 12b** using the device and materials properties shown in **Table 1**. It was assumed that the p-type and n-type legs have identical geometries. Using the equations derived in **Section 1.3.4**, the following device dimensions were used to arrive at the results*:* $l_p = l_n = l_s = 15\ mm$, $\tau = \tau_p = \tau_n = 75\ \mu m$ except otherwise stated, and $\tau_s = 70\ \mu m$.

Table 1: Properties of n-type and p-type thermoelements and substrate.

p-type material properties	
Seebeck Coefficient	220 μVK^{-1}
Electrical Resistivity	8.826 Ωm
Thermal Conductivity	1.472 Wm^{-1}K^{-1}
n-type material properties	
Seebeck Coefficient	-223 μVK^{-1}
Electrical Resistivity	8.239 Ωm
Thermal Conductivity	1.643 Wm^{-1}K^{-1}
Other properties	
Substrate thermal conductivity	0.2 Wm^{-1}K-1
Length of thermocouples	15 mm
Width of thermocouples	15 mm
Thickness of thermocouple	75 μm
Hot junction temperature	300 K

The material properties are identical to those found in another paper and for both p-type and n-type thermoelements they give a $ZT \sim 1$ at 300 K, which are typical values of ZT for current bulk materials on the market [5, 10]. If different material properties are used, both the *COP* and cooling power of the device will be higher if the material has a higher Seebeck coefficient. Also, a reduced electrical resistivity and thermal conductivity will lead to a better device performance.

In **Figure 12a**, the graph of q_c against I is given for the case of one thermocouple with a defined temperature of 300 K at the hot junctions and a thermoelement thickness of 75 μm. The dashed lines represent the performance that would have existed in the absence of any substrate, and hence are equivalent to the result of a bulk device with a thin cross-section. The solid lines represent the analytical solution obtained from the governing equations while taking the substrate thermal bypass into consideration. From the analytical solution, the maximum cooling power of the hybrid thermocouple at the stated operating conditions is 23.59 mW which is about 97% of that of a free-standing thermoelement. The scatter dots represent the numerical results, and from the graph can be observed that the error between the analytical results and the numerical results is minimal but increases with increasing current. This is probably due to the second term in **Equation 1.20,** which is the joule heating term that is proportional to the square of the current. According to **Equation 1.20**, half of the joule heat generated in a thermocouple flows to the cold junction while the remaining half goes to the hot junction. Since the cold junction temperature is lower than the hot junction temperature, the heat flux will be slightly greater toward the cold junction due to a higher temperature gradient, resulting

in the increasing difference between the analytical and numerical results for higher values of input current.

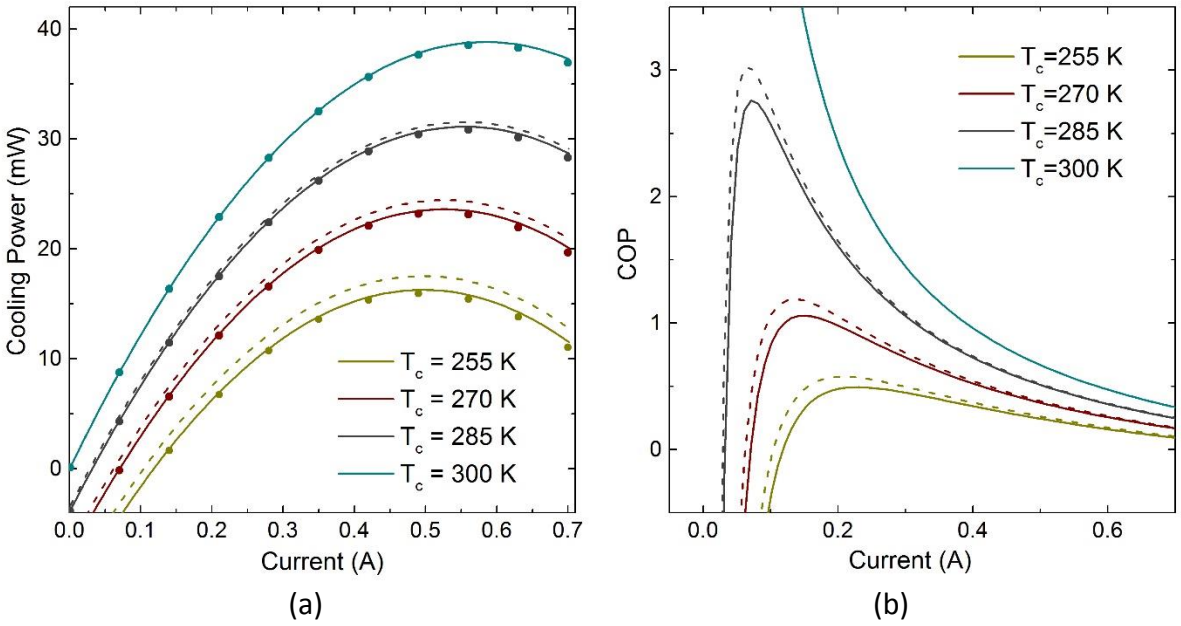

Figure 12: (a) q_C and (b) *COP* of a single thermoelectric couple as a function of current for different thermoelement thicknesses. In both cases the dashed line represents the performance of a free-standing device without the substrate. The scatter dots in (a) represent the numerical results.

In **Figure 12b** the relationship between *COP* and *I* is shown for different cold junction temperatures. In both **Figure 12a** and **Figure 12b**, for the ideal case without any conductive heat losses that represents T_c = 300 *K*, the substrate has no effect and the line that represents substrate-supported thermoelements is identical to results of a free-standing thermocouple. This is because at this theoretical maximum, the cold and hot junctions are at the same temperatures and therefore the net heat flux due difference in junction temperatures is zero.

Also it can be observed that maximum cooling power and *COP* for the thermocouple occurs at different currents. At a cold junction temperature of 270 *K*, maximum *COP* of the hybrid thermocouple is 1.06. For a representative bulk device with identical length and material properties, but with a cross-section of 3.5 *mm* by 3.5 *mm*, the maximum *COP* of the device is about 1.19. Thus, the maximum *COP* of the H-TEC couple is about 89% of that of such a representative bulk device. If the cold junction temperature is increased to 285 *K*, the maximum *COP* of the H-TEC couple will be 2.8, which will represent 93% of that of the representative bulk device.

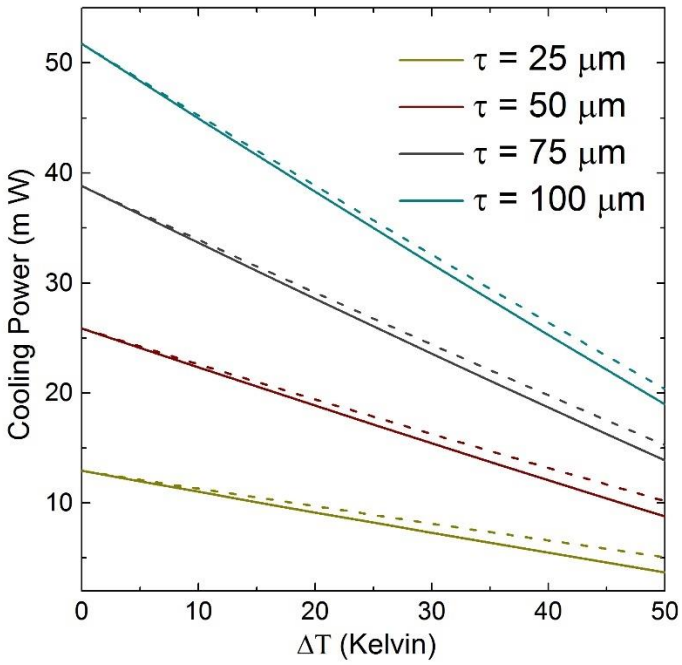

Figure 13: Maximum cooling power against the temperature difference across the device (ΔT) for different thermoelement thicknesses. The solid lines represent a substrate-supported theremoelectric films while the dashed lines represent free-standing films.

The maximized heat removal under optimized applied current that can be achieved for various temperature differences across one thermocouple is given in **Figure 13** for a number of thermoelectric element thicknesses. As with a bulk device, the cooling ability decreases with increasing temperature difference, because the H-TEC is required to pump heat across a larger temperature gradient. The cooling load is plotted for a thermocouple with a finite substrate thickness of 70 μm and an idealized zero substrate thickness. In this comparison, the two lines diverge as ΔT increases for each value of thermocouple thickness.

In **Figure 13** the vertical gap between a set of same-colored dashed and solid lines represent heat transfer losses due to thermal conduction through the substrate. At value of T_c = 275 *K*, which corresponds to a ΔT of 25 K, the loss in in q_c due to the substrate is only 2.6%. Also, the results indicates that even at values of T_c as low as 250 *K*, the percentage loss in performance can be low for relatively thick thermoelectric films. It should be noted that the vertical gap between the solid and dashed lines is approximately constant in each case, resulting in greater percentage loss for thinner thermocouples. The percentage loss associated with the substrate at a cold side temperature of 250 *K* is much greater for $\tau = 25\ \mu m$ than $\tau = 100\ \mu m$ where the percentage loss is approximately 28% and 7%, respectively. Thus, the use of thicker thermoelectric films is more advantageous in reducing the relative effect of the thermal bypass on q_C.

3.2. Overall Device Characteristics

As discussed above, the major difference between B-TEC and the H-TEC is the reduced fill-factor that was primarily a function of the active layer thickness (τ), the contact

area width (δ) and the corrugation angle (θ). The performance of the H-TEC can thus be explored primarily as a function of its geometrical properties by using equations presented in **Section 2.1** along with **Equation 1.20**. In this analysis, the module is considered to have an overall length $D = 20\ cm$ while the width is 1.5 *cm*. It is assumed that $\delta = 1.5\ mm$ and $\theta = 75^o$ except otherwise stated. All the material properties are identical to those stated in **Table 1**. For all the cases, **Equation 2.2** was used to calculate the number of thermocouples in a given length and the overall cooling power was then obtained from **Equation 1.20**. The performance results are provided in **Figure 14** and **Figure 15**.

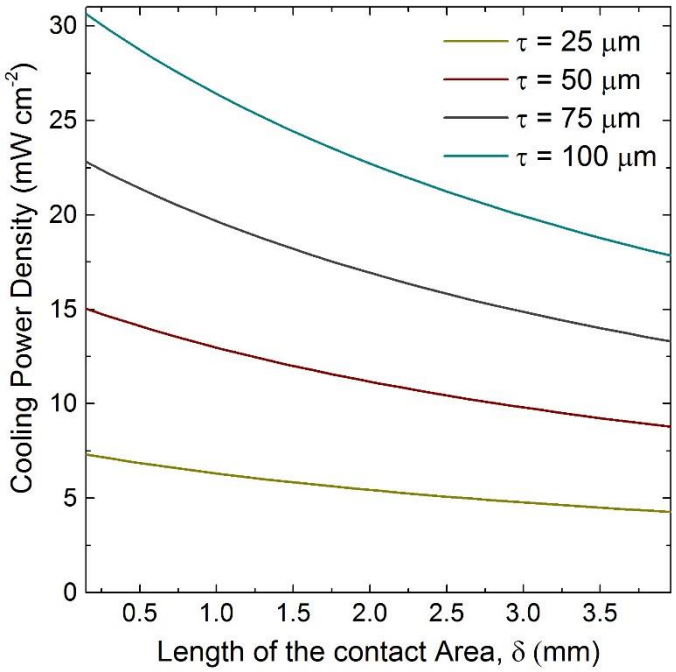

Figure 14: Cooling power of an array of thermcouples as a function of the length of the contact region.

Figure 14 shows the effect of varying the thermal contact region delta (δ). Reducing the length of the thermocouple contact area results in an increase in the cooling power density as more thermocouples can be packed into a given space. **Figure 15a** shows how the cooling power per unit area of the device varies with the angle of inclination of the legs (θ). The cooling power density against θ is initially almost linear but rises steeply as the angle approaches 90°. Therefore, for applications it is possible to match the required power density by carefully picking θ.

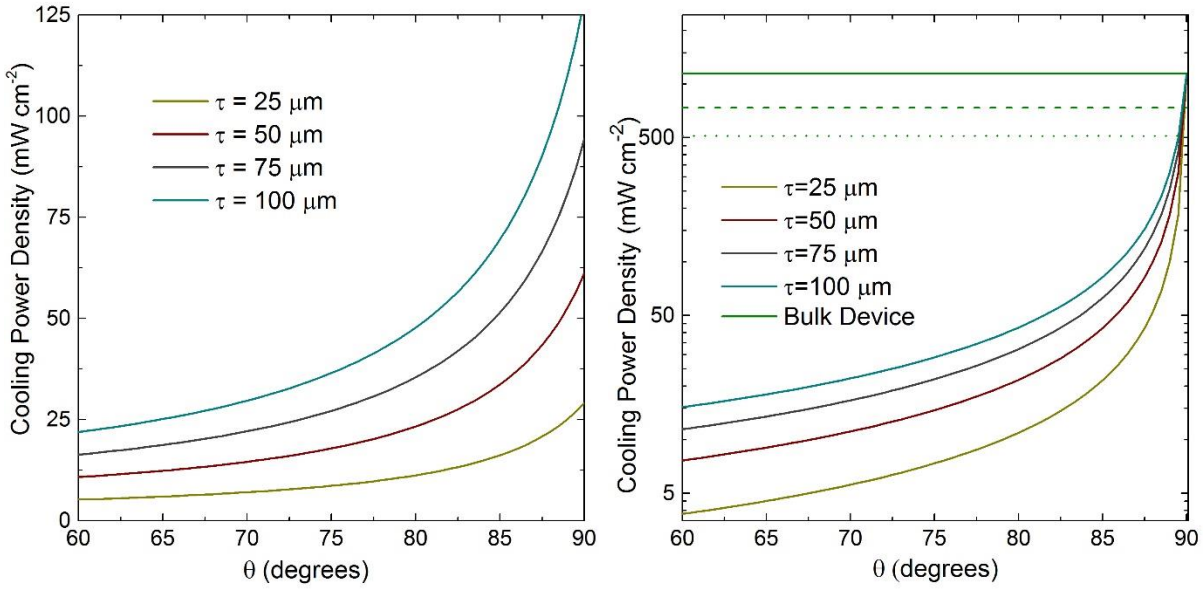

(a) (b)

Figure 15: (a) Cooling power density of an array of thermocouples as a function of the angle of inclination of the legs (δ = 1.5*mm*), (b) Cooling power density of an array of free-standing thermcouples as a function of the angle of inclination of the legs when δ = 2τ. The solid, dashed and dotted horizontal lines represent a spacing of 0, 0.75 *mm* and 1.5 *mm* respectively between the legs for a bulk device with a cross-section of 3.5 *mm* by 3.5 *mm*.

The purpose of **Figure 15b** is to compare the bulk and thick-film devices that have smaller or thinner cross-sections. Here, δ is set to twice the thickness of the device. Therefore, $\theta = 90^o$ corresponds to an idealized theoretical situation of zero spacing between closely stacked thick film thermocouples into a given length of the device, and all the devices compared are made to operate at their respective maximized Q_c. The horizontal lines in **Figure 15b** represent the performance of bulk thermoelements with the same material properties and length but with a cross-section of 3.5 *mm* by 3.5 *mm*.

The bulk array of thermocouples is assumed to be arranged within the same module area of D = 20 *cm* and a width of 1.5 *cm*, and it should be noted here that the width of the module is equal to the width of the thermoelements. Both the bulk and film thermoelements have equal lengths and the substrate effect is neglected for the thick film device. The point at which the horizontal lines cross the curved lines depict the angle of inclination required for the H-TECM to have an equivalent cooling power density to a bulk module. The line representing a bulk array of thermocouples with no spacing coincides with the thick film device at 90 degrees, which is tantamount to a theoretical no-space condition. This shows that if we slice a thick bulk thermoelement into thinner pieces and we neglect spacing and any parasitic heat loss mechanisms, the overall effect essentially remains the same if the devices operate at their respective maximized Q_c. It is also noticed that the dependence of Q_c on θ becomes more pronounced for higher values of θ. For instance, in **Fig 15a**, for a thermocouple thickness of 75 μm the value of Q_c increases by 35% when we increase θ from 60^o to 70^o as compared to a 60% increase when θ is increased from 70^o to 80^o.

3.3. H-TECM - Numerical Results

As stated in **Section 2.3**, two different computational models were built. Since the focus of this study is on the curved H-TEC with sinusoidal thermoelements (model 1), only the temperature distribution and the cooling power at the cold junction was generated for the model with flat legs (model 2). The total heat flux and the total electric field intensity is shown for the H-TEC in **Figure 16b** and **Figure 16c**.

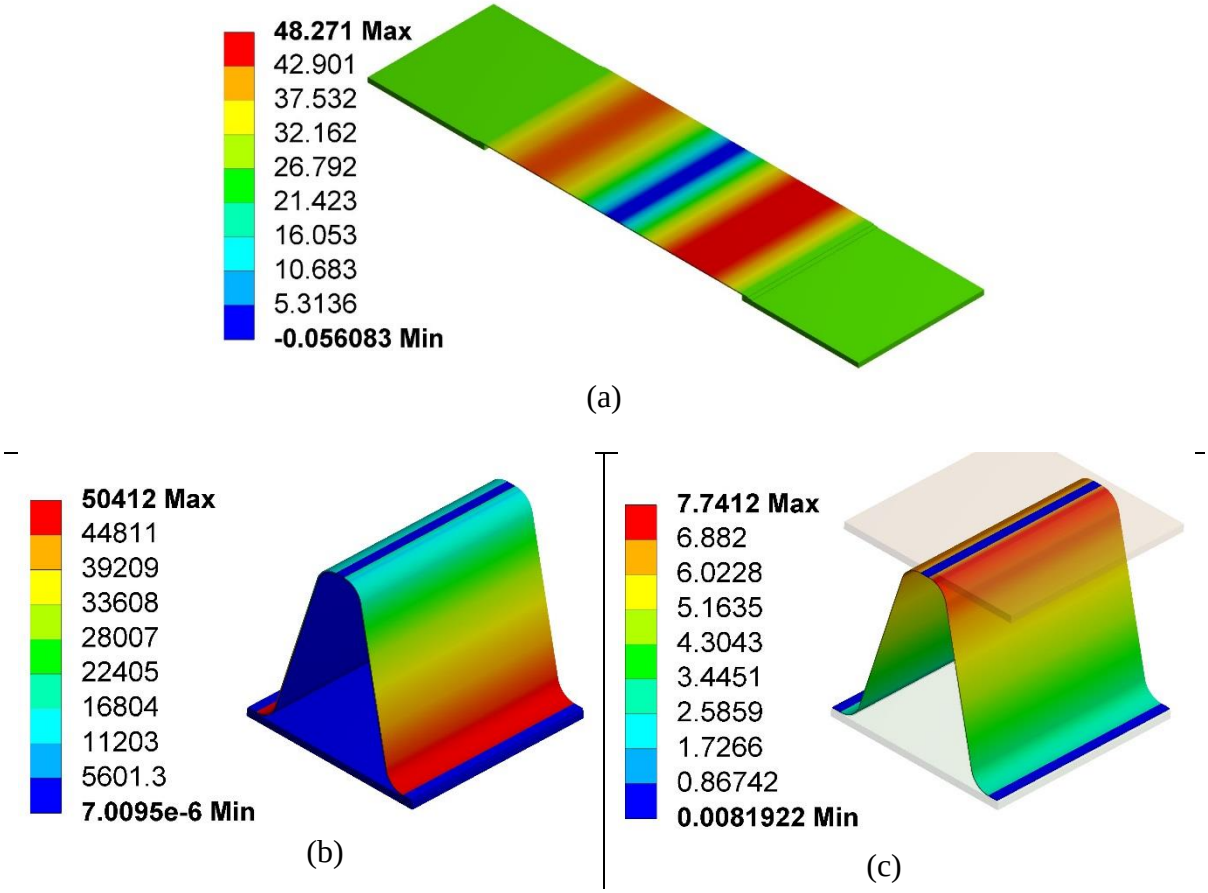

Figure 16: (a) the temperature profile in Kelvin for model 2 at an input current of I_{opt} = 0.5315 *A*, (b) the total heat flux in W/m^2 and, (c) total electric field intensity in V/m for model 1.

As expected, in **Figure 16b** the heat flux is higher at the hot junction than at the cold junction. This is expected as the hot junction temperature is higher than that of the cold junction, and so the absolute value of the Peltier heat released at hot junction is higher than the absolute value of the Peltier heat absorbed at the cold junction. On the other hand, the electric field intensity shown in **Figure 16c** reveals that electric potential is maximum at the cold junction and reduces as one moves towards the hot junction. This confirms prior discussion on the Seebeck effect, as the direction of temperature gradient between the ends of the device must be in an opposite direction to the electric potential.

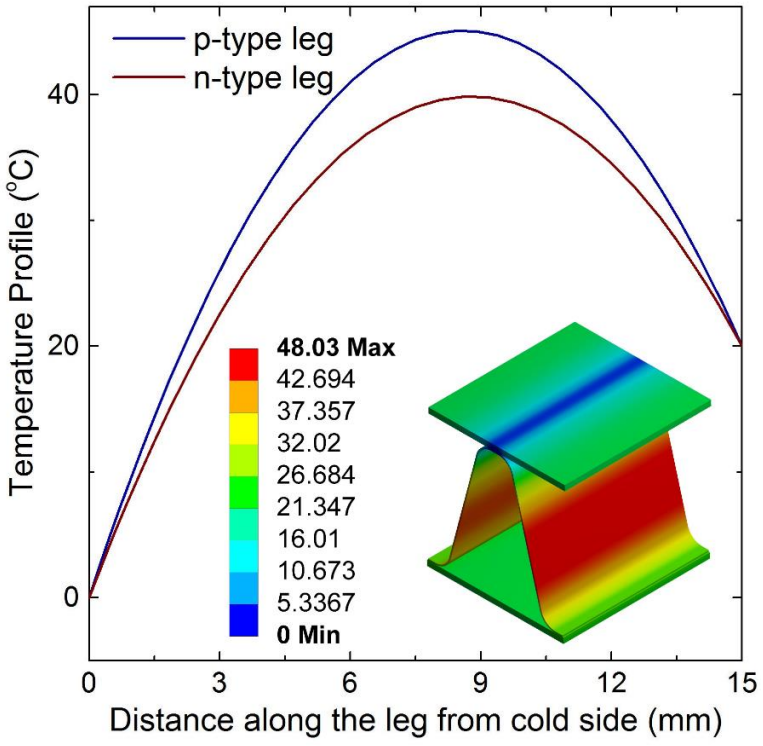

Figure 17: Temperature profile along the length of the thermocouple from cold junction to hot junction.

Figure 17 shows the temperature profile along the length of the legs, as obtained from the Model 1. A visual comparison between **Figure 16a** and **Figure 17** shows good agreement between the temperature profiles in both models, with a maximum approximately 48 ^{o}C and a minimum of approximately 0 ^{o}C in both cases. As expected, the maximum temperature does not occur exactly half way along the thermoelectric leg but is slightly closer to the hot junction due to a higher fixed boundary temperature at that junction. Also, the maximum temperature in the p-type thermoelement is higher than that in the n-type thermoelement, which is expected due to the higher electrical resistance of the p-type material.

The cooling power of the two models at different currents were also computed. In both cases, the current was varied from 0.1 A to 0.6 A and the cooling power at the cold junction was computed. The results are shown in a tabular form in **Table 2**. The results show that the cooling power of model 1 and model 2 are almost identical, suggesting that analytical results perfomed by assuming a flat TE film device are also valid for the hybrid themocouple

.

Table 2: The cooling power for the two numerical models at various input currents.

	Cooling Power (mW)	
Current (A)	**Model 1**	**Model 2**
0.1	3.8656	3.8995
0.2	12.545	12.587
0.3	18.944	18.999
0.4	23.062	23.135
0.5	24.899	24.996
0.6	24.455	24.582

3.4. Heat Sink Consideration

A key factor on the performance of thermoelectric devices is the ability to effectively drive heat toward and away from the device, for both heating and cooling applications. Since there is a maximum temperature difference above which a TE device will not function as expected, there is the need for elaborate heat fin designs to accompany the thermoelectric devices, such as the one shown in **Figure 18** [39, 40].

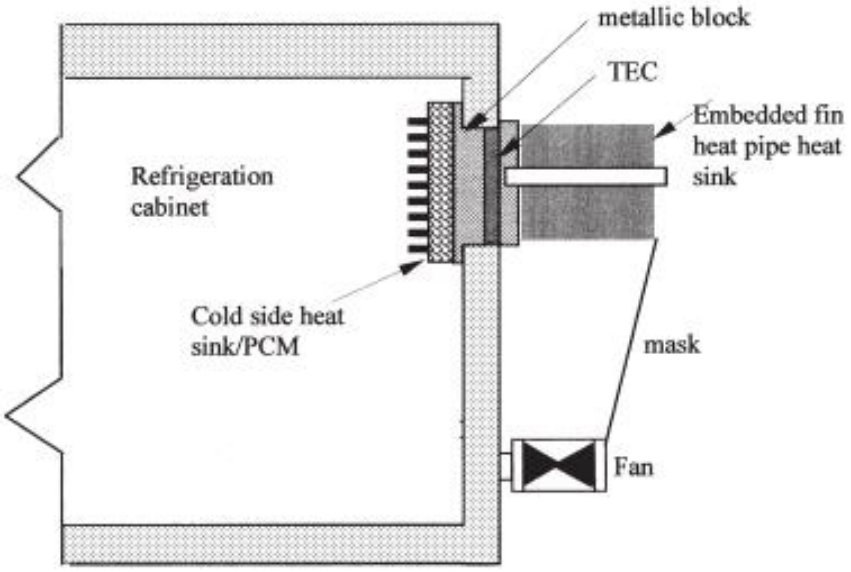

Figure 18: A diagram showing a typical bulk TE refrigeration device with its heat sink configuration.

Such heat sinks are designed to minimize thermal resistance either by utilizing forced convection or maximizing the exposed surface area [39]. One of the potential advantages of the H-TEC is in applications where a low cooling power density is required. For such applications, it will be better to use the sinusoidal device structure because the relatively large

area it already possesses. Forced convection may still be needed for the hot side because a larger heating load needs to be dissipated, consisting both the Peltier heat and the joule heat flux. However, the cold side may not require an extensive thermal management system. **Figure 19** shows the cooling power against the overall heat transfer coefficient at the cold side for both the B-TEC and the H-TEC. The bulk thermoelements have the same length of $l = 15mm$ as the H-TEC thermoelements but the dimensions of the cross-section is 3.5 *mm* by 3.5 *mm*. The number of thermocouples for the H-TEC and B-TEC are $n = 220$ and $n \simeq 20$ respectively, and this numbers were chosen such that the two modules produce the same cooling rate under identical cold side and hot side temperatures. The ambient temperature for the cold side and hot side were fixed at 273 *K* and 293 *K* respectively. Both modules being compared produce an approximately equal power of $Q_c = 5.27\ W$ for the boundary conditions of $T_c = 273\ K$ and $T_h = 308\ K$. In this case, a cold side temperature of 273 K corresponds to a cold side heat sink with an infinitesimal resistance.

Using a value of $\theta = 75^o$ and a reasonable spacing of 0.5 *cm* along the direction of the width of the thermoelements, the dimension of the area occupied by the H-TECM is approximately 400 cm^2. For the bulk module, using a spacing of 1 *mm*, the area occupied by the module is about 8.18 cm^2. It is assumed for both cases that we have an effective heat sink at the hot side which functions such that the temperature of the hot side is 308 ^oC for effective heat dissipation. Using **Equation 1.27** values of T_c corresponding to various values of overall heat transfer coefficient U were obtained and these cold side temperatures were used to determine the cooling power. For bulk modules, ceramic plates are usually used while planar plastic plates are used for the H-TECM, the later having thermal conductivity of 0.2 *W/mK* and

former having a typical thermal conductivity of 100 W/mK [49]. For typical thicknesses which are 500 μm and 1 mm for plastic planar plates and ceramic plates [50], the thermal resistance to heat flow across the plates are $2.75 \times 10^{-3}\ m^2K\ W^{-1}$ and $1\times10^{-4}\ m^2K\ W^{-1}$ for the H-TECM and the bulk module respectively. Thus for the sake of a fair comparison and because they are typically low, they are ignored in this analysis.

The result of this analysis is given in **Figure 19** and shows that the overall heat transfer coefficient needed to absorb a reasonable amount of heat when using the H-TEC is much lower compared to the B-TEC. To achieve a cooling rate which is 75% of the ideal case where we have an infinitesimal heat sink resistance, the overall heat transfer coefficient needed for the H-TEC and B-TEC are 7.6 W/m^2K and 375 W/m^2K respectively. In **Figure 19**, values of natural convection for air and water respectively for the H-TEC are shown, and these were calculated using a code written in MATLAB® (Mathworks Inc., Natick MA). The theoretical equations used to calculate the natural convection for air at the maximum Q_c of the H-TECM is shown in **Appendix A**, and the MATLAB code which utilizes an iterative procedure to arrive at the results is shown **Appendix B2**. The natural convection estimations were arrived at by assuming that the device is placed on its side such that the top and bottom plates form a vertical wall, and the values of air-cooled and water-cooled average heat transfer coefficients obtained for the H-TECM were 4.4 $Wm^{-2}K^{-1}$ and 120 $Wm^{-2}K^{-1}$ respectively. Air-cooled and water-cooled natural convection at the cold planar plate resulted in a cold junction temperature of 254 K and 271.9 K with the cooling being 63% and 98% of the ideal case where the thermal resistance at the cold side is infinitesimal, showing that an extensive management system may not be needed for the cold side. As presented in **Section 3.2**, as the angle of inclination of the legs (θ) increases

the power density of the device will increase, and therefore the requirement of a heat sink may be more probable. At reasonable angles of θ however, such as the angle of 75° used in this section, the density is low enough for such a device to be used without an elaborate heat sink design for the cold side.

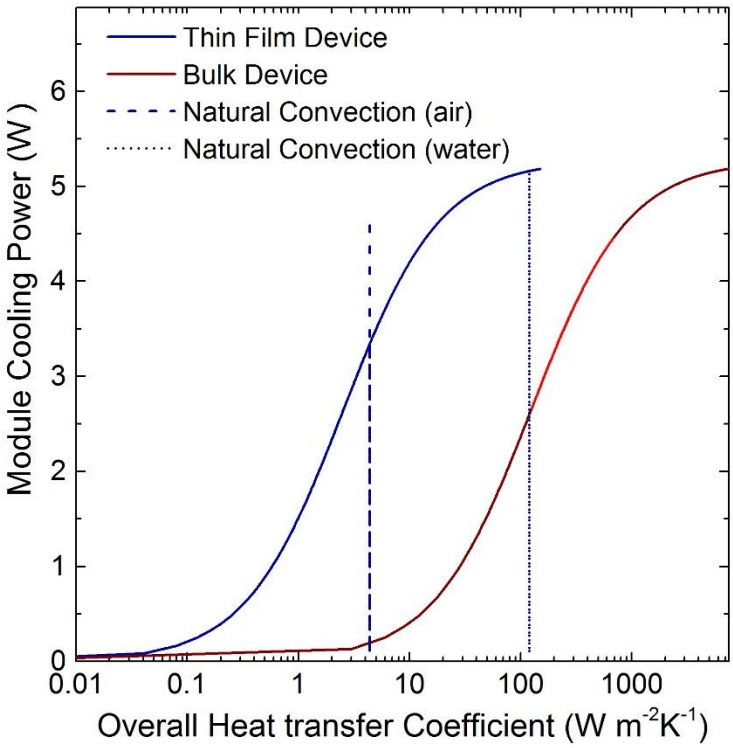

Figure 19: Cooling power of an array of thermocouples against the heat transfer coefficient at the cold side for both the hybrid module and a representative bulk module.

Therefore, in applications where a small amount of heat flux is dissipated over a relatively large area the H-TEC will perform better as it can give the same cooling power over a larger area, while lowering heat sink demands for either the cold side alone or both hot and

cold sides. Such applications may include situations involving body heat, electrical devices with low heat dissipation, or situations where a cold side heat sink is difficult to install.

3.5. Possible Applications of the H-TEC Design

In suggesting possible applications for the H-TE device, we must first consider the potential advantages of the device. First, the thick film TE elements may be solution processed in a roll-to-roll fashion into low-cost plastics substrates minimizing device costs. Furthermore, metal fins at the cold side and hot side may be unneeded reducing the total system cost. Also since its substrate is plastic and the extra weight of heat fins is not present, it will also be light-weight which improves portability. Finally, the plastic substrates and relatively thin thermoelectric materials may improve flexibility and durability of the elements. Considering all these factors, applications where this structure may have advantages over other cooling technologies such as B-TEC include body cooling applications, or applications where light-weight and portability is required.

The temperature of the human body is very important, because many processes in the human body depend on maintaining the body temperature at an optimum temperature [51]. Although sweating is a physiological process used to cool the body, other means of cooling may sometimes be necessary for comfort [34]. The average heat dissipated by the human body during normal conditions of body activity is about 7 mW/cm^2, but during exertive activities like running or other exercises, this value can be as high as 38 mW/cm^2 to 44 mW/cm^2 [51]. The human body, through various means acts as a thermostat to maintain the human body at approximately 37 ^oC, dissipating heat by convection, radiation and evaporation [51]. Thus, for

soldiers working in the desert, or workers in industries that have to work in a hot environment, a cooling device that can be integrated with clothing and other worn accessories can be of immense importance [34]. As mentioned earlier, such a device must be lightweight – not adding considerable weight to the body. In addition to this, for body cooling applications it must not be sensitive to rapid movements or perturbations. The H-TEC can be of use in such applications because of its suitability in satisfying these conditions, and also because by reversing the direction of current flow, the cooling device can be changed to a heating device for use in cold weather conditions. In situations where there is a lot of solar radiation available, the H-TE device can be powered by solar cells.

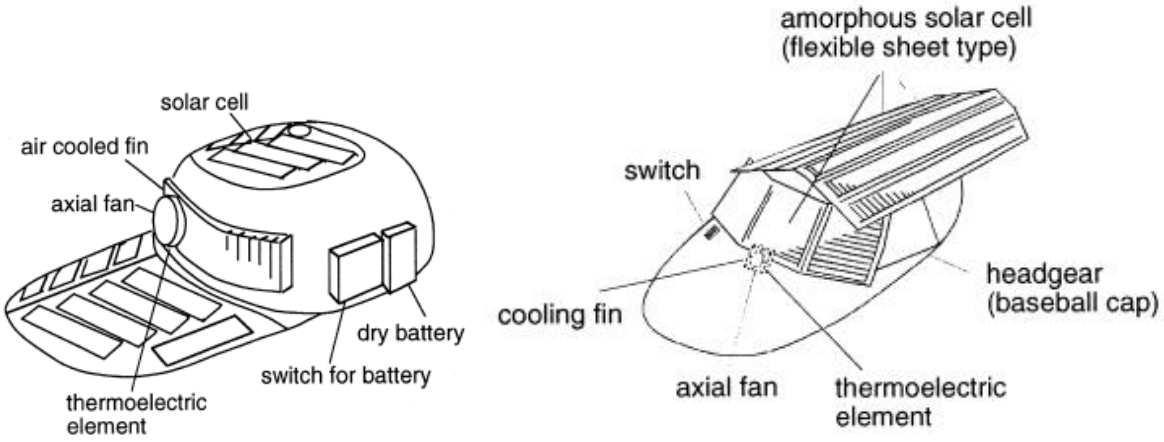

(a) (b)

Figure 20: Two prototypes of a thermoelectrically cooled headgear. (a) is powered using crystalline solar cells while (b) is powered using flexible solar cells (Ref [33]).

The use of bulk thermoelectric materials for a body cooling application powered by solar cells has been explored by Hara, et al., where the cooling performance a solar-powered

head-gear prototype was evaluated [33]. Three different models were analyzed and two of the three configurations are shown in **Figure 20**. The first model uses a crystalline solar cell while the other one uses an amorphous or flexible organic solar cell, and these were tested for different cases using subjects for the activities of sitting, waking, and cycling [33]. It was concluded that model B was a better option due to lighter weight, and for thermal comfort and it was recommended that the cooling temperature should be between 4 ^{o}C to 5 ^{o}C below the body temperature [33]. This therefore presents a representative example, showing the sort of applications where the H-TEC may be suitable. Such a headgear described will need to be lightweight and will benefit from the low heat sink requirements of the H-TEC.

4. Conclusion and Future work

4.1. Conclusion

In this thesis a novel TE device structure has been presented, which involves the use of thermoelectric films printed on plastic substrates which have the shape of a sinusoid. We have also shown that the parasitic heat losses of such a device will be minimal. The cooling power density of the device can be controlled by carefully choosing the angle of inclination of the device and how sharp-pointed the contact regions are. In comparison with a representative bulk device used in this study, the new device structure produces a similar *COP* but a lower cooling power density. Therefore, such a device will also be very useful in cases where we have a large area but a relatively small cooling load. In these cases, the novel device structure presents the advantages of being more cost effective in spreading out its cooling and potentially significantly reducing heat sink demands.

A major limiting factor in TE implementation has been the cost of the thermoelectric elements. While a thermoelectric figure of merit (ZT) values of 2.4 have been obtained for n-type Bi_2Te_3/Sb_2Te_3 superlattices at room temperature, the high costs of materials and processing are prohibitive [5, 12, 52]. Alternatively, thick film processing methods of thermoelectric materials, such as screen-printing have been explored. Screen printing has the advantage of much quicker processing time and cheaper production cost, and the H-TEC can benefit from such processing techniques. The films produced have been found to be of similar properties to their bulk counterparts [42, 53, 54]. Thus, due to lower heat sink demands, the employment of low cost plastic materials and potentially cheap and quicker manufacturing

methods, the hybrid design has the potential to be cheaper than bulk thermoelectric devices. It should be noted that the application of this device is restricted to relatively low temperature applications given the desire to employ low cost plastic substrate materials.

4.2. Future Work

As indicated in **Section 2.2**, certain assumptions were made in this study, one of which is that the device operates in a vacuum, which makes it reasonable to ignore convection. It was also assumed that the temperatures are relatively low, which is reasonable considering the temperature limit imposed upon such a device by the use of plastic substrates. Future work will need to evaluate the influence of natural convection and radiation on the performance of the device. The use of a partial vacuum may be useful if it does not reduce performance appreciably, as this may present lower manufacturing costs.

Also, the device is still in the earlier stages of development, and effort is being made to build the first prototype of the device. In the development of a physical model to prove the concept presented in this thesis, a number of pitfalls have to be avoided. First, care has to be taken in designing contact regions. Heat is absorbed and released at the junctions of the two materials and not along the entire length of the materials. This means that in the absence of convection and radiation, heat is conducted through the cold plastic plate into the cold junction, and from the hot junction through the hot side plate into the heat sink. Since conduction requires a medium to occur, there must be physical contact between the junctions and the flat plates at both hot and cold sides.

In addition to this the melting point of the plastic must be taken into consideration. Since plastics are amorphous materials, they do not possess a definite melting point like crystalline materials and therefore melting occurs over a range. Also, as seen in the results in **Section 3.3**, the maximum temperature usually occurs not at the hot side, but somewhere in between the two junctions of the device due to joule heating. In practical implementation of such a device, care must be taken by designing for the junction temperatures such that the maximum temperature does not to exceed the temperature at which bonds begin to break and mechanical strength of the device begins to wane.

Also, the mechanical joints in the device has to be properly fastened. Such a thermoelectric device will be required to undergo several cycles of repeated heating and cooling. The plastic materials used must be able to withstand such repeated thermal stresses without cracking and ultimate failure, and the plastic substrate in particular must also endure such stresses without detaching from the top or bottom plates.

Finally, this work has laid the foundation by theoretically and numerically characterizing the H-TEC design. The practical limit of some parameters have to be quantified. For instance, the use of a thin substrate is desirable, but thinness of the substrate is limited by the requirement that the substrate must be strong enough to support the device. This work as evaluated the rate of heat absorption at the cold junction. In practice, this value will be slightly lesser than the predicted amount because of an additional thermal resistance of the top plate. To reduce this drop in performance, the top and bottom plates should be made as thin as possible, but again the thinness that can be achieved will be limited by the requirement that the top and bottom plates must be mechanically strong enough. In addition to this, there may be

practical limits to the angle of inclination of the legs due to manufacturing constraints or increased probability of failure as the angle of inclination increases. Many of this constraints will be needed to be evaluated experimentally by future work, in evaluating the potentials of the hybrid thermoelectric device.

REFERENCES

[1]` J. Paulo and P. Gaspar, "Review and future trend of energy harvesting methods for portable medical devices," in *Proceedings of the World Congress on Engineering*, 2010.

[2] H. W. Hillhouse and M. T. Tuominen, "Modeling the thermoelectric transport properties of nanowires embedded in oriented microporous and mesoporous films," *Microporous and Mesoporous Materials,* vol. 47, no. 1, pp. 39-50, 2001.

[3] M. Naji, M. Alata and M. Al-Nimr, "Transient behaviour of a thermoelectric device," in *Proceedings of the Institution of Mechanical Engineers, Part A: Journal of Power and Energy*, 2003.

[4] D. M. Rowe, CRC handbook of thermoelectrics, CRC press, 1995.

[5] T. M. Tritt, "Thermoelectric Materials: Principles, Structure, Properties, and Applications," in *Encyclopedia of Materials: Science and Technology*, Elsevier Science Ltd., 2002.

[6] W.-H. Chen, C.-Y. Liao and C.-I. Hung, "A numerical study on the performance of miniature thermoelectric cooler affected by Thomson effect," *Applied Energy*, vol. 89, no. 1, pp. 464-473, 2012.

[7] A. McGaughey, "Modeling thermoelectric materials and devices," *American Ceramic Society Bulletin,* vol. 91, no. 3, pp. 34-38, 2012.

[8] S. Riffat and X. Ma, "Thermoelectrics: a review of present and potential applications," *Applied Thermal Engineering* , vol. 23, no. 8, pp. 913-935, 2003.

[9] Y. G. Gurevich and G. N. Logvinov, "Physics of thermoelectric cooling," *Semiconductor Science and Technology*, vol. 20 , no. 12, pp. R57-R64, 2005.

[10] H. Lee, "The Thomson effect and the ideal equation on thermoelectric coolers," *Energy,* pp. 61-69, 2013.

[11] F. J. DiSalvo, "Thermoelectric cooling and power generation," *Science* , vol. 285, no. 5428, pp. 703-706, 1999.

[12] R. Venkatasubramanian, E. Siivola, T. Colpitts and B. O'Quinn, "Thin-film thermoelectric devices with high room-temperature figures of merit," *Nature,* vol. 413, no. 6856, pp. 597-602, 2001.

[13] G. Min and D. Rowe, "Cooling performance of integrated thermoelectric microcooler," *Solid-state Electronics* , vol. 43, no. 5, pp. 923-929, 1999.

[14] Y. Zhang, Y. Chen, C. Gong, J. Yang, R. Qian and Y. Wang, "Optimization of superlattice thermoelectric materials and microcoolers," *Journal of Microelectromechanical Systems,* vol. 16, no. 5, pp. 1113-1119, 2007.

[15] J. Sharp, J. Bierschenk and J. Hylan B. Lyon, "Overview of solid-state thermoelectric refrigerators and possible applications to on-chip thermal management," *Proceedings of the IEEE* , vol. 94, no. 8, pp. 1602-1612, 2006.

[16] K. Fukutani and A. Shakouri, "Optimization of thin film microcoolers for hot spot removal in packaged integrated circuit chips," in *22nd Annual IEEE Semiconductor Thermal Measurement and Management Symposium*, Dallas, TX, MAR 14-16, 2006.

[17] L. Goncalves, "The Deposition of Bi2Te3 and Sb2Te3 Thermoelectric Thin-films by Thermal Co-Evaporation and Applications in Energy Harvesting".

[18] A. J. Gross, G. S. Hwang, B. Huang, H. Yang, N. Ghafouri, H. Kim, R. L. Peterson, C. Uher, M. Kaviany and K. Najafi, "Multistage Planar Thermoelectric Microcoolers," *Journal of Microelectromechanical Systems* , vol. 20, no. 5, pp. 1201-1210, 2011.

[19] G. Min, D. Rowe and F. Volklein, "Integrated thin film thermoelectric cooler," *ELECTRONICS LETTERS* , vol. 34, no. 2, pp. 222-223, 1998.

[20] F. Volklein, G. Min and D. Rowe, "Modelling of a microelectromechanical thermoelectric cooler," *Sensors and Actuators A-physical* , vol. 75, no. 2, pp. 95-101, 1999.

[21] Z.-H. Jin, "Buckling Of Thin Film Thermoelectrics," *International Journal of Fracture* , vol. 180, no. 1, pp. 129-136, 2013.

[22] L. W. da Silva and M. Kaviany, "Micro-thermoelectric cooler: interfacial effects on thermal and electrical transport," *International Journal of Heat and Mass Transfer,* vol. 47, no. 10, pp. 2417-2435, 2004.

[23] I.-Y. Huang, J.-C. Lin, K.-D. She, M.-C. Li, J.-H. Chen and J.-S. Kuo, "Development of low-cost micro-thermoelectric coolers utilizing MEMS technology," *Sensors and Actuators A: Physical,* vol. 148, no. 1, pp. 176-185, 2008.

[24] G. Hwang, A. Gross, H. Kim, S. Lee, N. Ghafouri, B. Huang, C. Lawrence, C. Uher, K. Najafi and M. Kaviany, "Micro thermoelectric cooler: Planar multistage," *International Journal of Heat and Mass Transfer,* vol. 52, no. 7, pp. 1843--1852, 2009.

[25] J.-P. Fleurial, A. Borshchevsky, M. Ryan, W. Phillips, J. Snyder, T. Caillat, E. Kolawa, J. Herman, P. Mueller and M. Nicolet, "Development of thick-film thermoelectric microcoolers using electrochemical deposition," in *MRS Proceedings,* 1998.

[26] T. M. Tritt, "Thermoelectric phenomena, materials, and applications," *Annual review of materials research,* vol. 41, pp. 433-448, 2011.

[27] A. Shakouri, "Recent developments in semiconductor thermoelectric physics and materials," *Materials Research,* vol. 41, no. 1, p. 399, 2011.

[28] M. Hamid Elsheikh, D. A. Shnawah, M. F. M. Sabri, S. B. M. Said, M. Haji Hassan, M. B. Ali Bashir and M. Mohamad, "A review on thermoelectric renewable energy: Principle parameters that affect their performance," *Renewable and Sustainable Energy Reviews,* vol. 30, pp. 337-355, 2014.

[29] Z. Tian, S. Lee and G. Chen, "A Comprehensive Review of Heat Transfer in Thermoelectric Materials and Devices," *arXiv preprint arXiv:1401.0749,* 2014.

[30] D. Zhao and G. Tan, "A review of thermoelectric cooling: Materials, modeling and applications," *Applied Thermal Engineering,* vol. 66, no. 1, pp. 15-24, 2014.

[31] D. Astrain, A. Martínez and A. Rodríguez, "Improvement of a thermoelectric and vapour compression hybrid refrigerator," *Applied Thermal Engineering,* vol. 39, pp. 140-150, 2012.

[32] S. Abdul-Wahab, A. Elkamel, A. M. Al-Damkhi, I. h. A. Al-Habsi, H. S. Al-Rubai'ey, A. K. Al-Battashi, A. R. Al-Tamimi, K. H. Al-Mamari and M. U. Chutani, "Design and experimental investigation of portable solar thermoelectric refrigerator," *Renewable Energy,* vol. 34, no. 1, pp. 30-34, 2009.

[33] T. Hara, H. Azuma, H. Shimizu, H. Obora and S. Sato, "Cooling performance of solar cell driven, thermoelectric cooling prototype headgear," *Applied Thermal Engineering,* vol. 18, no. 11, pp. 1159-1169, 1998.

[34] R. Bansevičius, R. Račkienė and J. A. & Virbalis, "The body cooling system integrated into the clothes," *Electronics and Electrical Engineering.--Kaunas: Technologija,* no. 5, p. 77, 2007.

[35] J. Carmo, M. Silva, J. Ribeiro, R. Wolffenbuttel, P. Alpuim, J. Rocha, L. Goncalves and J. Correia, "Digitally-controlled array of solid-state microcoolers for use in surgery," *Microsystem technologies,* vol. 17, no. 8, pp. 1283-1291, 2011.

[36] H.-S. Choi, S. Yun and K.-i. Whang, "Development of a temperature-controlled car-seat system utilizing thermoelectric device," *Applied Thermal Engineering,* vol. 27, no. 17, pp. 2841-2849, 2007.

[37] [Online]. Available: http://www.gentherm.com/page/interior-heating. [Accessed March 2014].

[38] [Online]. Available: http://www.gentherm.com/page/thermal-management-applications. [Accessed March 2014].

[39] S. Riffat, S. Omer and X. Ma, "A novel thermoelectric refrigeration system employing heat pipes and a phase change material: an experimental investigation," *Renewable Energy,* vol. 23, no. 2, pp. 313-323, 2001.

[40] H. Lee, "Optimal design of thermoelectric devices with dimensional analysis," *Applied Energy,* vol. 106, pp. 79-88, 2013.

[41] R. McCarty, "A comparison between numerical and simplified thermoelectric cooler models," *Journal of electronic materials,* vol. 39, no. 9, pp. 1842-1847, 2010.

[42] H. B. Lee, J. H. We, H. J. Yang, K. Kim, K. C. Choi and B. J. Cho, "Thermoelectric properties of screen-printed ZnSb film," *Thin Solid Films,* vol. 519 , no. 16, pp. 5441-5443, 2011.

[43] X.-D. Wang, Y.-X. Huang, C.-H. Cheng, D. Ta-Wei Lin and C.-H. Kang, "A three-dimensional numerical modeling of thermoelectric device with consideration of coupling of temperature field and electric potential field," *Energy,* vol. 47, no. 1, pp. 488-497, 2012.

[44] S. B. Riffat and X. Ma, "Improving the coefficient of performance of thermoelectric cooling systems: a review," *International journal of energy research,* vol. 28, no. 9, pp. 753-768, 2004.

[45] M. Cosnier, G. Fraisse and L. Luo, "An experimental and numerical study of a thermoelectric air-cooling and air-heating system," *International Journal of Refrigeration,* vol. 31, no. 6, pp. 1051-1062, 2008.

[46] M. Russel, D. Ewing and C. Ching, "Characterization of a thermoelectric cooler based thermal management system under different operating conditions," *Applied Thermal Engineering* , vol. 50, no. 1, pp. 652-659, 2013.

[47] H. S. Lee, "Thermal design: heat sinks, thermoelectrics, heat pipes, compact heat exchangers, and solar cells," 2010.

[48] B. J. Huang, C. J. Chin and C. L. Duang, "A design method of thermoelectric cooler," *International Journal of Refrigeration,* vol. 23, no. 3, pp. 208--218, 2000.

[49] T. Yang, J. Xiao, W. Zhao and Q. Zhang, "Structural optimization of two-stage thermoelectric generator for wide temperature range application," in *Electric Information and Control Engineering (ICEICE), 2011 International Conference on*, 2011.

[50] S. Lineykin and S. Ben-Yaakov, "PSPICE-Compatible Equivalent Circuit of Thermoelectric Cooler," 2005.

[51] V. Leonov and R. Vullers, "Wearable thermoelectric generators for body-powered devices," *Journal of electronic materials,* vol. 38, no. 7, pp. 1491-1498, 2009.

[52] J. H. We, S. J. Kim, G. S. Kim and B. J. Cho, "Improvement of thermoelectric properties of screen-printed Bi2Te3 thick film by optimization of the annealing process," *Journal of Alloys and Compounds,* vol. 552, pp. 107-110, 2013.

[53] A. Tsuyoshi and M. Ohmukai, "Electrodeposition of Bi-Sb Alloy Using Cu electrodes," *Materials Sciences and Applications,* vol. 3, pp. 492-494, 2012.

[54] S. J. Kim, J. H. We, J. S. Kim, G. S. Kim and B. J. Cho, "Thermoelectric properties of P-type Sb2Te3 thick film processed by a screen-printing technique and a subsequent annealing process," *Journal of Alloys and Compounds,* vol. 582, pp. 177-180, 2013.

[55] A. Bejan, Heat Transfer, John Wiley & Sons, Inc, 1993.

APPENDICES

Appendix A. Natural Convection on an Isothermal, vertical Wall

The following shows analysis shows a partial derivation of the heat transfer coefficient when natural convection occurs over a vertical isothermal wall which has been presented in Ref [55]. In this case, the average heat flux across the wall is given by,

$$\bar{q} = \frac{\overline{Nu}.\Delta T.k}{H} \qquad (A1.1)$$

$\overline{Nu}$ represents the height-averaged Nusselt number and *Nu* is called the Nusselt number and is the ratio of conductive to convective heat transfer across the boundary. *Nu* is given by,

$$Nu = \frac{hy}{\sigma_f} \qquad (A1.2)$$

h is the local heat transfer coefficient. Also, ΔT is the difference in temperature between the surface of the wall and the ambient fluid temperature outside the thermal boundary layer. σ_f is the thermal conductivity of the fluid, while *H* is the height of the wall.

When heat transfer occurs across a solid-fluid boundary in natural convection, for an isothermal solid wall,

$$Nu \propto Ra_y^{0.25}. \qquad (A1.3)$$

Ra_y is a dimensionless number known as the Rayleigh Number and is given by,

$$Ra_y = \frac{g\beta\Delta T H^3}{\alpha_T \nu}. \qquad (A1.4)$$

In the above equation, g is the acceleration due to gravity, β is the coefficient of volumetric expansion, α_T is the thermal diffusivity and ν is the kinematic viscosity of the fluid.

The local Nusselt number is given as a function of Prandtl number and Rayleigh number as,

$$Nu_y = 0.503\left(\frac{Pr}{Pr + 0.986Pr^{0.5} + 0.492}\right)^{0.25} Ra_y^{0.25}. \qquad (A1.5)$$

In order to find the average heat transfer rate from the solid boundary it is useful to find the average Nusselt number by integrating the local Nusselt number over the entire height and dividing by the height. Thus, the average Nusselt number is given by:

$$\overline{Nu}_y = 0.671\left(\frac{Pr}{Pr + 0.986Pr^{0.5} + 0.492}\right)^{0.25} Ra_y^{0.25}. \qquad (A1.6)$$

Since the Prandtl number of most fluids is temperature dependent, the height-averaged Nusselt number is a function of temperature for most fluids and should be taken into account in an analysis. However, for air the Prandtl number is fairly constant at 0.72 for a relatively wide temperature range. Therefore the height-averaged Nusselt number is given by,

$$\overline{Nu}_y = 0.517\, Ra_y^{0.25}. \qquad (A1.7)$$

The average heat transfer coefficient can therefore be obtained from the average Nusselt number using the following,

$$\bar{h} = \frac{\overline{Nu}_y\, k}{H}. \qquad (A1.8)$$

Appendix B. MATLAB Codes

B1. Determining the cooling power of the H-TEC device as a function of θ

```
%-------------------------------------------------------------%
% To calculate the cooling power of a hybrid TE device       %
%   as a function of angle inclination of the legs           %
%-------------------------------------------------------------%
%                  Opeoluwa Owoyele                           %
%           North Carolina State University                   %
%-------------------------------------------------------------
fileID=fopen(HTE.txt','w');
% material properties
    delta= 0.0015;
    theta=75;
    RhoP=0.000008826;
    RhoN=0.000008239;
    Cp=1.472;
    Cn=1.643;
    Cs=0.20;
    AlphaP=0.00022;
    AlphaN=-0.000223 ;
%%%%%%%%%%%%%%%%%%%%%%%%%%

%Device Properties
    tau = 0.000075;
    ts = 0.000070;
    W = 0.015;
    L = 0.015;
    Rhoc=0; %contact resistance is negelected.
    Alpha= AlphaP-AlphaN;
    A = W*tau;
    Rc=Rhoc/A;
    Ks=2*Cs*ts*W/L;
    Th=300;
    Kt=(Cp+Cn)*tau*W/L;
    Rt=(RhoP+RhoN)*L/(W*tau);
    K=Kt+Ks;
    R=Rt+Rc/2;
    I=Alpha*Tc/R; %operates at optimum current.
    Tc=273;
%%%%%%%%%%%%%%%%%%%%%%%%%%

fprintf(fileID,'%12s %12s %12s %12s\n','theta','qc','n','TQc');
for theta=60:2:90
    cosn=cos(pi*theta/180);
    cot=1/tan(pi*theta/180);
    sn=sin(pi*theta/180);
    lamda=L-(delta+tau*(cot-1));
    DD=0.2; %DD is the total length of array of themocouples.
```

```
        n=DD/2/(delta+lamda*cosn-tau*sn);
        Qh=((I*Alpha*Tamb)-(K*(Tamb-Tc))+(0.5*I*I*R))/(1-I*Alpha*Hh+K*Hh);
        Th=300;
        W=Alpha*I*(Th-Tc)+I*I*R;
        qc=((I*Alpha*Tc)-(K*(Th-Tc))-(0.5*I*I*R));
        COP=qc/W;
        DTmax=(Alpha^2)*(Tc^2)/(2*R*K);
        TQc=n*qc;
        DT=Th-Tc;
        RS=[theta;qc;n;TQc];
        fprintf(fileID,'%12.8f %12.8f %12.8f %12.8f\n',RS);
    end
```

B2. Air-cooled natural convection and cooling power along an isothermal vertical wall bounded at the other side by a thermoelectric device.

```
%-------------------------------------------------------------%
%       Cooling power of an H-TEC with air-cooled             %
%         natural convection on the cold plate                %
%-------------------------------------------------------------%
%                  Opeoluwa Owoyele                           %
%           North Carolina State University                   %
%-------------------------------------------------------------%
%material properties
    RhoP=0.000008826;
    RhoN=0.000008239;
    Cp=1.472;
    Cn=1.643;
    Cs=0.2;
    AlphaP=0.00022;
    AlphaN=-0.000223;
%%%%%%%%%%%%%%%%%%%%%%%%%%%%%

%device properties
    tt = 0.000075;
    ts = 0.000070;
    W = 0.015;
    L = 0.015;
    Rhoc=0;
    Tinfh=293;
    Tinfc=273;
    Alpha= AlphaP-AlphaN;
    A = W*tt;
    Rc=Rhoc/A;
    Ks=2*Cs*ts*W/L;
    Kt=(Cp+Cn)*tt*W/L;
    Rt=(RhoP+RhoN)*L/(W*tt);
    K=Kt+Ks;

    R=Rt+Rc/2;
```

```
    Tc=Tinfc;
%%%%%%%%%%%%%%%%%%%%%%%%%%
%operational characteristics
    Th=308;
    Iopt=Alpha*Tc/R;
    Tcold=263;
    Thold=283;
    hcold=0;
    hhold=0;
    n=0;
    n1=220; %number of thermocouples
    At=0.04; %total area of device
%%%%%%%%%%%%%%%%%%%%%%%%%%%%%%%%%
%Omega Data: omega is g*beta/alpha/nu
    omega=[367,148,125,107,90.7,57.1];
    Omega=omega*10^6;
    kc=[0.02, 0.024,0.025,0.025,0.026,0.028];
    Tfc=0.5*(Tc+Tinfc);
    Tfh=0.5*(Th+Tinfh);
    error=5;

%begin iterative procedure to find hc
for i=1:50
I=Alpha*Tc/R;
n=0;
    while (n <= 100)

    Tfc=0.5*(Tc+Tinfc);
    Tfh=0.5*(Th+Tinfh);

        if (Tfc < 273) && (Tfc >= 223)
        x=(Tfc-233)/(273-233);
        omeg = x*(Omega(2)-Omega(1))+ Omega(1);
        kcc=x*(kc(2)-kc(1))+kc(1);

        elseif (Tfc < 283) && (Tfc >= 273)
        x=(Tfc-283)/(293-283);
        omeg = x*(Omega(3)-Omega(2))+ Omega(2);
        kcc=x*(kc(3)-kc(2))+kc(2);

        elseif (Tfc < 293) && (Tfc >= 283)
        x=(Tfc-283)/(293-283);
        omeg = x*(Omega(4)-Omega(3))+ Omega(3);
        kcc=x*(kc(4)-kc(3))+kc(3);

        else
        end
```

```
    hc=(0.517*kcc/0.2*(omeg*0.2^3*(Tinfc-Tc))^0.25)*At;
    Hc=hc/At;
    Tc=(hc*Tinfc+n1*(0.5*I^2*R+K*Th))/(n1*(I*Alpha+K)+hc);
    errorTc=abs(Tc-Tcold);
    errorhc=abs(hc-hcold);
    errorhh=abs(hh-hhold);
    error=errorTc+errorhc+errorhh;
    Tcold=Tc;
    hcold=hc;
    hhold=hh;
    n=n+1;
    end

error=error;
Hc=Hc;
Qc=((I*Alpha*Tc)-(K*(Th-Tc))-(0.5*I*I*R));
TQc=n1*Qc;
end

error
Hc
Qc=((I*Alpha*Tc)-(K*(Th-Tc))-(0.5*I*I*R))
TQc=n1*Qc
```